TUDelft

Delft University of Technology

Numerical parametric study of radio wave soil treatment for pathogen suppression

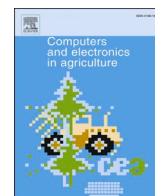Sturm, G.S.J.; van der Wurff, A.; Linnenbank, S.; Bonnet, J.; Koppert, A.

Important note
To cite this publication, please use the final published version (if applicable).
Please check the document version above.

Numerical parametric study of radio wave soil treatment for pathogen suppression

G.S.J. Sturm [a,*], A. van der Wurff [b], S. Linnenbank [c], J. Bonnet [d], A. Koppert [c]

[a] *Process & Energy department, Delft University of Technology, Leeghwaterstraat 39, 2628 CB Delft, the Netherlands*
[b] *Groen Agro Control, Distributieweg 1, 2645 EG Delfgauw, the Netherlands*
[c] *Koppert Machines B.V., Vlotlaan 616, 2681 TX Monster, the Netherlands*
[d] *Stichting Control in Food & Flowers, Distributieweg 1, 2645 EG Delfgauw, the Netherlands*

A B S T R A C T

Radio wave treatment for pathogen suppression in glasshouse horticulture may become an alternative to steam treatment. It has several advantages, but it also requires further development before it can replace steam treatment. In a previous study we developed a numerical modeling approach to aid this development. In this present study, the modeling approach is used to study the radio wave treatment process and to explore strategies for improvement. A parametric study is performed to develop insight into the effect of several environmental and process parameters on the radio wave treatment process, and a comparison is made to steam treatment.

1. Introduction

The use of fossil fuels becomes progressively less desirable. Consequently, for contemporary energy intensive applications, alternative technologies are explored that do not require fossil fuels. One such application is radio wave treatment of soil in open soil glasshouse horticulture. The current practice is to use steam to treat soil for pathogen suppression. In particular, a sheet is placed over the soil, and steam is injected underneath it, thereby being applied to the soil for an extended period of time to raise temperature to suppress pathogens (Dabbene, et al., 2003). This is an energy intensive process that requires in the order of about five cubic meters of natural gas per square meter of soil, or an equivalent amount of fuel oil. Furthermore, it is a labor intensive process too, so any opportunity for automation is much desired.

An alternative approach is to use a renewable form of electricity as energy source for soil heating. To this end, a radio wave treatment prototype called Agritron (Koppert Machines, 2014; Fig. 1) has been developed by Koppert Machines B.V.; the thermographic image that is included with the photograph shows the operation of the device through the trail of heated soil that is left behind the prototype as it drives over it. The prototype vehicle carries a 100 kW 915 MHz generator that feeds into an antenna that directs the radio wave energy into the soil. There this energy is dissipated into heat, which causes a temperature increase that is sufficient to suppress pathogens.

This treatment process has a large degree of complexity. It starts by propagation and dissipation of electromagnetic energy. This causes heat generation and increased vapor pressure in soil, which both induce primary transport phenomena of heat and moisture. In addition, the treatment may cause release and transport of nutrients. Finally, the increased temperature can eliminate, inactivate or otherwise affect organisms in or on soil. The ultimate outcome of these biological effects does not necessarily relate in a plain monotonic relation to the treatment intensity, as will be illustrated in Section 1.1 below.

This present study is a follow-up of our prior study (Sturm, et al., 2023). In that study we reported on the development of a framework for numerical simulation of the radio wave treatment process. This framework is ultimately intended to aid and accelerate the design of both equipment and treatment methods. The primary simulation environment for this model is Comsol Multyphysics 5.5 (COMSOL AB, 2019) which is combined with Matlab (The Mathworks, 2019). It was developed to run on workstation grade hardware so that it can be used as a tool to develop insight into the treatment process, and to aid the design of treatment protocols.

The focus of the simulation framework as it has been developed so far is on the physical interactions of,

- the propagation and dissipation of the electromagnetic field; and
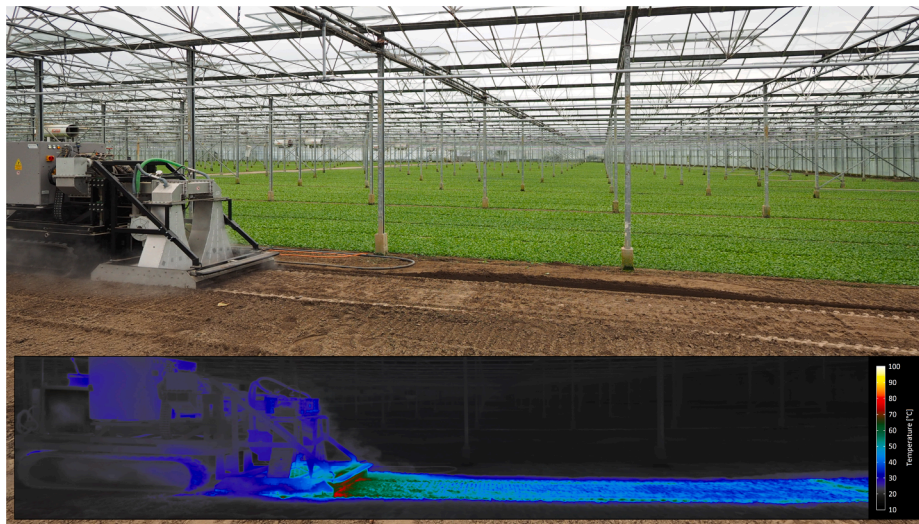

Fig. 1. Agritron prototype in operation; thermogram captured with FLIR A655sc with 24.6 mm T197922 lens (Sturm, et al., 2023, reprinted with permission).

- the transport phenomena, which are associated with electromagnetic heat generation and the redistribution of heat and moisture that are induced by heat generation.

The simulation framework model was not intended to provide at the outset an accurate prediction of the effectiveness of the treatment process. At present, many of the physical and biological parameters that govern the physical and biological processes in soil are unknown. For now, this limits the precision to which the treatment process can be replicated through numerical simulation. Moreover, insufficient insight is available into the set of biological processes that comprise the soil biosystem, and their response to radio wave heating. Therefore, at present, in order to facilitate interpretation of the simulation results, only a basic placeholder model is implemented for biological effects.

The currently feasible scope that is available for simulation is macroscopic evaluation of the physical variables outlined above. This present study performs such evaluation through a parametric study of physical and treatment parameters. In this manner, the study explores the development of treatment methods. A distinction is made here between the design of *soil treatment equipment* versus the design of *treatment methods*. Analogously to the culinary context, a microwave oven needs to be paired with a recipe in order to produce a meal. Similarly, a soil treatment system needs the development of treatment protocols before it can be applied effectively. This present study therefore initiates this protocol development by exploring the relation between treatment effectiveness and the physical parameters that affect it.

1.1. Background

The concept of pathogen suppression in soil with electromagnetic energy has first been proposed in the mid-twentieth century. A preliminary study by Eglitis et al. (1956) report on the suppression on Pythium in soil through an oven-type device at a frequency of 27 MHz. A decade later, Seaman and Wallen (1967) report on the suppression of several seed-borne pathogens by application of a radio frequency field at a frequency of 59 to 94 MHz, and several years later, Eglitis and Johnson (1970) present a follow-up study on their earlier preliminary study, in which they apply a 27 MHz field to several soilborne pathogens, among which Fusarium, Pythium, Rhizoctonia, and Rhizobium. A year later, O'Bannon and Good (1971) explore the ultra-high frequency band, through the application of a 2450 MHz microwave field to *M. incognita*. This is followed by a study by Barker et al. (1972), who apply the 2450 MHz frequency to several plant pathogenic nematode species. Nelson and Stetson (1974) perform a comparative study between the VHF and UHF frequency bands of 39 MHz and 2450 MHz respectively. They report on controlling an insect species, i.e. Rice Weevils (*S. oryzae*), and they conclude that treatment with the lower 39 MHz band shows better potential for selective heating of insects than the 2450 MHz band. Up to this point, the studies that are mentioned here use oven/heater-type devices that could be used in a laboratory setting to evaluate the effect of an electromagnetic field on a pathogen species in a laboratory setting. In contrast Menges and Wayland (1974) and Wayland et al. (1975) report on experimentation with a custom microwave applicator that radiates a 2450 MHz field onto a bed of soil. Both studies report on the effectiveness of this treatment for weed control.

What this overview of early studies shows, is that there is a variety of design choices available with respect to the frequency and applicator types. This variety is mirrored in the later emergence of similar research efforts into soil remediation by means of electromagnetic fields. The early studies in this context congregate around a variety of the lower frequency bands that are applied via stationary electrodes into soil, in particular Edelstein et al. (1994) at 6.78 MHz, Blanchard et al. (1996) at 6.78 MHz, Dev and Sresty (1996) at 6.78 MHz and 27.13 MHz, and Avila et al. (1996) at 13.56 MHz and 27.12 MHz. Later work on remediation shifts attention mainly to higher frequencies, in particular to the microwave frequency of 2450 MHz, as is illustrated by the review of Falciglia et al. (2018). Though much work is performed in ubiquitous microwave heating cavities, they present several concept for microwave applicators that are more tailored to a particular application.

The utilization of electromagnetic fields either for soil disinfestation or for soil remediation are related in the sense that both applications ultimately aim to apply considerable amounts of electromagnetic energy to large volumes of soil. The engineering challenges are similar, and both fields of research exhibit a similar trend in the popularity of the 2450 MHz microwave frequency in studies. In particular, the search interface of Science Direct (2024) returns comparable numbers of search results for the combinations "microwave *and* soil" versus "radio frequency *and* soil", for the search period up to the 1990s. After that period, the search term "microwave" becomes approximately five times more popular than "radio frequency". It would appear that microwave heating – almost exclusively understood to be application of the 2450 MHz frequency – is driven by the familiarity and availability of microwave heating equipment. The suitability of this particular frequency for food preparation, though, ought not automatically imply its superiority for soil treatment. Its suitability would depend on the particular requirements of each specific treatment case. Several frequencies are available for heating applications, known as ISM frequencies (Industrial Scientific and Medical) as defined by the International

Telecommunication Union (2020). Frequency selection would best be determined by specific design requirements, and not so much by familiarity with or availability of particular equipment. In the two microwave frequency (300 MHz–300 GHz) bands of 915 MHz and 2450 MHz there are notable differences in efficiency, maximum available power, and treatment depth of magnetron based generators. With respect to efficiency, these are 60–70 % resp. 80–90 %, while for maximum power these are 6 kW resp. 100 kW (Meredith, 1998) (corroborated by personal communication with representative of Sairem SAS, M. Radoiu, 2011). Regarding the treatment depth, the maximum effective reach can be derived (Pozar, 2005) under certain medium simplifications to scale with the inverse of the frequency. Hence at 915 MHz, the potential treatment depth would be approximately three times deeper than at 2450 MHz.

What this expanded discussion on frequency boils down to in the context of our study, is that a degree of apprehension needs to be maintained while considering pre-existing data for implementation in a computer simulation of the radio wave treatment process, despite the fact that a considerable volume of information already exists in literature. This motivates our decision to use ad interim a basic placeholder model for biological processes in our simulation. Incidentally, we have a report in preparation on the development of an experimental system that provides replication in a laboratory setting of the treatment conditions in soil as applied by the Agritron prototype. We envision this as a means to develop models that closely match the biological processes that occur in soil during treatment.

Despite the present limitations, much information can already be found in literature. A review by Nelson (1996) includes several works on soil disinfestation by electromagnetic heating, almost all of which involve 2450 MHz, with only a few at 27 MHz or 40 MHz bands. In his review, the author includes a study by Ferriss (1984), in which it is mentioned that microwave energy is effective, though only at small scale, which illustrates the limitations of the 2450 MHz frequency band. This does not preclude, however, exploration of this frequency band, as for a subset of applications, the higher frequency may be beneficial. Some examples will be pointed out below where the shallower treatment effect would be beneficial. Moreover, the accessibility of this frequency band has enabled researchers to steadily expand the knowledge base on disinfestation by application of radio frequency or microwave fields over time, as will be illustrated by the following overview.

Mavrogianopoulos et al. (2000) explore the temperature development that is achievable in soil. Velázquez-Martí and Gracia-López (2004) present a design for an applicator to transmit electromagnetic energy onto large soil surfaces, and they include a simulation of the electromagnetic field in this design. Sartorato et al. (2006) present a study on weed control; Rahi and Rich report on control of nematodes (Rahi & Rich, 2007; Rahi & Rich, 2011); Komarova et al. (2008) present a study on inactivation of soil bacteria. A special note has to be made on the efforts of Brodie and co-workers, who have been particularly active in the field of suppression of pathogens, microorganisms, and plants. They report on soil pasteurization, and controlling ryegrass, seeds and weeds (Brodie, et al., 2007a; Brodie, et al., 2007b). In particular with respect to their studies on suppressing surface plants, the shorter wavelength and shallower penetration depth may actually be preferrable, as these concentrate heat effects to the surface where it is desired (Brodie, et al., 2007c; Brodie, et al., 2012a; Brodie, et al., 2012b). The group has also generated several studies on treatment of soil, to assess the effect on the microbial population, the yield of wheat and on bacteria in soil (Brodie, et al., 2015; Khan, et al., 2016; Khan, et al., 2019). They also present a design for a comb-type slow wave applicator for weed and pathogen control, and assess its energy demand (Brodie, et al., 2019). They also present a towed prototype for treatment of the soil surface in a field (Brodie, et al., 2020a; Brodie, et al., 2022). Bringing our attention to other researchers, Şahïn (2014) reports on the germination rates of cress and arugula seeds, a low exposure resulted in increased germination as compared to no exposure, while a higher dosage

decreased it. This accentuates that biological processes are more complex than can be expressed through plain monotonic trends. Further studies report on: the inhibition of seed germination (Wilde, et al., 2017); the bioavailability of nutrients (Abbey, et al., 2017); the mutation breeding of chrysanthemum (Miler & Kulus, 2018); and the effects on diverse bacterial populations (Li, et al., 2023). Several studies on numerical simulation with a focus on physical processes have also been published. This includes a study by on the FDTD method to simulate the electromagnetic and thermal responses that occur during the treatment process (Fanti, et al., 2017); a simulation of a horn antenna for soil treatment in CST Studio Suite, and experimental verification of the results by exposure of grapes in soil (Sabry, et al., 2018); and simulation of the treatment process in Comsol Multiphysics (Sun, et al., 2021; Sun, et al., 2022). As pointed out above, these articles explore the 2450 MHz frequency band. More recent studies, however, have been shifting attention to lower frequencies again. Tkalec et al. (2009) have investigated the effects on onions of exposure to 400 MHz and 900 MHz fields. Tadigiri et al. (2016) present a study on suppression of root knot nematodes by 13.27 MHz and 40 MHz fields. Maynaud et al. (2019) report on the physicochemical and biological properties of soil in response to exposure to a 915 MHz field. Hess et al. (2018, 2019) report on seedling suppression with a 915 MHz field. Finally Brodie et al., (2020b) report on the development of a new applicator type, i.e. a slow-wave comb-type applicator, both in the 2450 MHz and in the 922 MHz frequency bands.

Valuable insight can be obtained not only from studies that involve the application of electromagnetic fields to induce heating. Studies that involve conventional heating can also have relevance, since they describe responses to temperature exposure that are equally applicable to thermal effects that are electromagnetically caused. For example both Warcup (1951) and Bollen (1969) mention the release of organic matter due to steam treatment that may ultimately be detrimental and facilitate reinfestation. The notion that more heat does not necessarily result in less pathogens is also found in the book on soil solarization edited by Katan and Devay (1991a). In one of their own contributions Katan and DeVay (1991b) they mention non-monotonic and interdependent interactions and the need to avoid "disturbing the biological balance". Their co-contributors Griffin and Baker (1991) and Chen et al. (1991) speak more graphically of "the boomerang effect" in which poorly dosed treatment creates an opportunity for pathogens to reestablish and reinfest. In the context of steam treatment, Roux-Michollet et al. (2010) hypothesize that the slow acting nature of the treatment may allow time for bacteria to employ survival mechanisms against the elevated temperature. This would then also result in reinfestation. What this suggests, is that not only the thermal dose needs to be considered, but also the dynamics in which it is applied.

Another aspect of radio wave treatment with potential dynamic considerations is the integration with the electrical power grid. As the power consumption can in principle be flexibly adjusted, radio wave treatment could possibly be considered as a demand response application. In such application the consumption can be controlled such that it is used to stabilize the power grid (Conchado et al., 2012). This may provide access to favorable energy prices on short term electricity markets, specifically the intraday market and imbalance market (Welle, 2016; Agro Energy, 2017).

1.2. Study objectives

The main question that this study explores is: how does variation of physical parameters affect the treatment outcome? The study is outlined as follows in several sub-topics:

- First a systematic parametric study is performed to evaluate the sensitivity of the treatment to variation of the individual parameters. These comprise of:
  - porosity variation;
  - application of pre-drying of soil in preparation to treatment;

- variation of composition in terms of humidity and salinity;
- variation of transport parameters: Darcy permeability and thermal conductivity;
- variation in power application, which is relevant in the context of integration with the electrical power grid.
- This is followed by a simulation to verify whether the simulation is able to replicate temperature and pressure profiles that were measured during field trials with the prototype.
- Finally, a simulation of the conventional treatment method of soil steaming is performed, so that radio wave treatment can be juxtaposed against steam treatment.

This introductory section is followed by two sections that present the simulation methodology: Section 2 summarizes the simulation framework that was reported in our prior study, while Section 3 presents modifications made to the model to enable simulation of steam treatment.

The subsequent four sections present simulation of the particular sub-topics as outlined above. These sections each present both results and brief discussion of their respective simulations:

- Section 4 presents the base case simulation,
- Section 5 presents simulation of systematic variation of individual parameters with respect to the base case,
- Section 6 confirms that the simulation framework can indeed approximate temperature and pressure measurements that were obtained through prototype trials, and lastly,
- Section 7 presents simulation of the steam treatment process of soil.

Section 8 provides a more in-depth discussion on the juxtaposition of radio wave treatment against steam treatment. Finally, Section 9 summarizes the findings in conclusions.

2. Simulation methodology

This section presents a concise overview of the modeling approach. Please refer to our previous work (Sturm, et al., 2023) for a detailed model description. The model geometry comprises of a horn antenna as described by Meredith (1998) traveling over a body of soil. Symmetry is used to halve the simulated domain. The dimensions of the simulated soil domain are 3 m long, 0.6 m wide (width of the simulated half), and 0.5 m deep. The model is solved in three steps:

- First a three-dimensional simulation is performed that involves the radio wave antenna and a soil volume underneath it. Refer to simulation results, for example to Fig. 4 to Fig. 9 in Section 4, for a graphic representation of the simulated geometry. In this first step, the electromagnetic field and transport phenomena are included. An advection velocity u_0 is imposed on the soil volume to represent the relative movement of the antenna relative to the soil.
- In the second step, only the long term transport phenomena are considered. The transport phenomena over these time scales are invariant along the direction of motion of the antenna, which permits a two-dimensional simulation in this step. The former step and this second step are performed in COMSOL Multiphysics as simulation environment.
- In the third step, the data is exported to MATLAB to calculate the response of a simple pathogen model in the vertical plane perpendicular to the direction of motion.

From the requirement to use the model for design purposes, the condition follows that the model be suitable for workstation grade computational hardware. Therefore, the mesh quality for the simulation cannot be set sufficiently high to avoid numerical instabilities due to Runge's Oscillations that are induced by the imposed advection in the soil domain. Instead, these oscillations are suppressed by diffusive stabilization applied as,

$$\alpha_s \nabla^2 \widehat{V} + \widehat{V} = V \tag{1}$$

where V is an arbitrary variable, and $\alpha_s = 6.25 \cdot 10^{-6}$ m^2 is the diffusive smoothing parameter. This results in a smoothing effect with a characteristic length of $\sqrt{6.25 \bullet 10^{-6}} = 2.5 \bullet 10^{-3}$ meter. This is acceptable, because this length is smaller than the macroscopic variations that this study considers. The caret distinguishes the smoothed variable from the non-smoothed one.

2.1. Transport phenomena

Transport of heat and moisture in the soil are described via a number of diffusion equations. The soil domain contains two homogeneous and fully overlapping domains of different phase that interact with each other. These domains are the solid/liquid domain, and the gas/vapor domain. The former accounts for,

- the temperature of the solid/liquid domain T_{sl}, and
- the volumetric molar bulk density of liquid water n_{wl}

The second domain accounts for the transport phenomena in gas and vapor phase, which is expressed by the following variables,

- the temperature of the gas/vapor domain T_{av},
- the volumetric molar bulk density of water vapor n_{wv}, and
- the gas/vapor pressure p

The variables n_{wl} and n_{wv} are defined with respect to the bulk soil volume, i.e. the total of solid and liquid volume and the porous volume in soil.

A first order process is imposed to describe heat and vapor transfer between the two domains of different phase. A characteristic length for this process of $\beta_v = 10$ mm is found to be the shortest length that can be applied without the occurrence numerical instability. A time constant τ_v is defined through division with the antenna speed,

$$\tau_v = \beta_v / u_0 \tag{2}$$

A function f_A defines the Antoine equation that is parametrized according to the NIST Chemistry Webbook (2018) that provides the equilibrium vapor pressure for water versus temperature,

$$p_v = f_A(T_{sl}) \tag{3}$$

With Equations (2) and (3), and the ideal gas law (R represents the gas constant), an expression is formulated for the volumetric rate of evaporation from the solid/liquid domain to the gas/vapor domain,

$$r_v = \left(\frac{p_v \varphi}{R T_{sl}} - \frac{n_{wv} + \widehat{n}_{wv}}{2} \right) \frac{1}{\tau_v} \tag{4}$$

The symbol φ in Eq. (4) represents the porous volume fraction for gas and vapor in the soil. This evaporation process extracts heat from the solid/liquid phase domain according to,

$$Q_v = r_v \left[M_w \left(\left(T_{sl} - T_{H_{v,0}} \right) \left(C_{p,wv} - C_{p,wl} \right) + H_{v,0} \right) + M_w C_{p,wv} (T_{av} - T_{sl}) \right] \tag{5}$$

here $T_{H_{v,0}}$ is a reference temperature of 10 °C at which the enthalpy of evaporation of water $H_{v,0}$ is 2477 kJ/kg (The Engineering Toolbox, 2010). The parameters $C_{p,wv}$ and $C_{p,wl}$ represent the specific heat of water vapor and liquid water respectively (1870 J/kgK (The Engineering Toolbox, 2005) resp. 4180 J/kgK (The Engineering Toolbox, 2003d)); M_w represents the molecular mass of water, 18 g/mol. Transfer of sensible heat between the phase domains is defined as,

$$Q_{\Delta T} = (T_{sl} - T_{av})(M_w C_{p,wv} n_{wv} + M_a C_{p,a} n_a)\frac{1}{\tau_v} \tag{6}$$

The symbol M_a is the molecular mass of air (29 g/mol, The Engineering Toolbox (2004a)); n_a is the volumetric molar bulk density of air in soil, defined in the same manner as n_{wv}; $C_{p,a}$ is the heat capacity of air (1006 J/(kg·K) The Engineering Toolbox (2004b)).

The diffusion processes that govern the transport of the aforementioned variables are described by the following partial differential equations:

- Transport of heat in the solid/liquid domain (T_{sl}),

$$\partial_t T_{sl}(\rho_s C_{p,s} + M_w C_{p,wl} n_{wl}) + \nabla \bullet - \kappa \nabla T_{sl} + (\rho_s C_{p,s} + M_w C_{p,wl} n_{wl})\overline{u}_0$$
$$\bullet \nabla T_{sl} + \frac{\kappa}{\alpha_s} T_{sl}$$
$$= \frac{\kappa}{\alpha_s} T_{sl} - Q_v - Q_{v,bc} - Q_{\Delta T} + Q_{RF} \tag{7}$$

- The diffusion of volumetric molar liquid water density (n_{wl}),

$$\partial_t n_{wl} + \nabla \bullet (-\alpha_w \nabla n_{wl}) + \overline{u}_0 \bullet \nabla n_{wl} + \frac{\alpha_w}{\alpha_s} n_{wl} = -r_v - r_{v,bc} + \frac{\alpha_w}{\alpha_s}\widehat{n}_{wl} \tag{8}$$

- Transport of heat in the gas/vapor domain (T_{av}),

$$(M_w C_{p,wv} n_{wv} + M_a C_{p,a} n_a)\partial_t T_{av} + \nabla$$
$$\bullet - \kappa_{av} \nabla T_{av} + (M_w C_{p,wv} n_{wv} + M_a C_{p,a} n_a)\left(\frac{k}{\mu\varphi}\nabla p - \overline{u}_0\right)$$
$$\bullet \nabla T_{av} + \frac{M_w C_{p,wv} n_{wv} + M_a C_{p,a} n_a}{\tau_v} T_{av}$$
$$= \frac{M_w C_{p,wv} n_{wv} + M_a C_{p,a} n_a}{\tau_v} T_{sl} \tag{9}$$

- Transport of water vapor (n_{wv}),

$$\partial_t n_{wv} + \nabla \bullet - \alpha_v \nabla n_{wv} - \left(\frac{k\nabla p}{\mu\varphi} - \overline{u}_0\right)\bullet \nabla n_{wv} - \frac{k\nabla^2 p}{\mu\varphi} n_{wv} = r_v \tag{10}$$

- Pressure p in the gas/vapor domain (p),

$$\partial_t p + \nabla \bullet - \frac{k\widehat{p}}{\mu\varphi}\nabla p + \left(\frac{kp}{\mu\varphi}\frac{\nabla T_{sl}}{T_{sl}} + \overline{u}_0 - \frac{k}{\mu\varphi}\nabla\widehat{p}\right)\bullet \nabla p - \left(\frac{\nabla T_{sl}}{T_{sl}}\right.$$
$$\left.\bullet \overline{u}_0 + \frac{\partial_t T_{sl}}{T_{sl}}\right)p$$
$$= \frac{T_{sl}R}{\varphi} r_v \tag{11}$$

The physical phenomena that govern the transport phenomena are diffusion and flow through a porous medium. The latter follows Darcy's law and is characterized by a permeability parameter. In order to avoid confusion, in this work it is termed "Darcy permeability" in order to differentiate it from "magnetic permeability", which is also included in this text.

These differential equations are presented in coefficient form as proscribed by the Partial Differential Equations (PDE) interface of Comsol Multiphysics. Table 1 lists the transport parameters and source terms included in Equations (7) to (11) that yet remained to be specified at this point.

A more detailed discussion on the model for transport phenomena is

Table 1
Transport parameters and source terms.

Symbol	Description	Value	Reference
ρ_s	soil density	1500 kg/m^3 (dry)	Mills (1999), Bear (1972)
		1800 kg/m^3 (wet)	
$C_{p,s}$	heat capacity of dry soil	1900 J/kgK (dry)	Mills (1999), Bear (1972)
		2280 J/kgK (wet)	
κ	soil thermal conductivity	1 W/mK (dry)	Mills (1999)
		2 W/mK (wet)	
$Q_{v,bc}$	heat of evaporation due to evaporation to surroundings, volumetrically imposed near the soil surface		Sturm et al. (2023), Section 4.4.4
$r_{v,bc}$	rate of evaporation due to evaporation to surroundings, volumetrically imposed near the soil surface		Sturm et al. (2023), Section 4.2
Q_{RF}	volumetric heating due to radio wave exposure		Present study, Section 2.2
α_w	diffusivity of liquid water in soil	temperature dependent interpolation function	Staple (1965)
k	Darcy permeability	10^{-9} cm^2 (base case)	Bear (1972)
μ	viscosity of air and vapor	15 μPa·s	The Engineering Toolbox (2003b, 2004c)
α_v	diffusivity of water vapor in air	0.28 cm^2/s	Wikipedia (2019)
κ_{av}	thermal conductivity of air/ vapor	24.35 mW/mK	The Engineering Toolbox (2003c)

provided by our prior study (Sturm, et al., 2023). This includes the derivation of the diffusion equations and the boundary equations.

2.2. Electromagnetics

The radio wave field is simulated with the RF-module of Comsol Multiphysics. This module applies Maxwell's electromagnetic field equations as the wave equation for time harmonic fields,

$$\nabla \times (\mu_r^{-1}\nabla \times \mathbf{E}) - k_0^2 \varepsilon_r \mathbf{E} = 0 \tag{12}$$

In this equation $\mathbf{E}$ is the electric field vector component of the radio wave field. The soil under consideration has no particular magnetic properties. Therefore, the relative magnetic permeability equates to unity, $\mu_r = 1$. Electromagnetism only depends on the relative dielectric permittivity ε_r, which varies with soil composition and temperature. A dielectric model that accounts for variation of porosity, humidity, salinity, and temperature is applied. This model extrapolates data from dielectric properties measurement of glasshouse horticulture soil samples measured with an Agilent 85070E kit with performance probe option connected to an Agilent E5071C network analyzer and an Agilent N4691B ECal module. The term k_0 is the free space wave number at the operating frequency (915 MHz) of the Agritron,

$$k_0 = \frac{\omega}{c_0} = \omega\sqrt{\varepsilon_0\mu_0} = \frac{5.75 \bullet 10^9 \text{rad/s}}{299.8 \bullet 10^6 \text{m/s}} = 19.18 \text{rad/m} \tag{13}$$

The symbols ω, c_0, ε_0, and μ_0 represent respectively: the angular the angular frequency of the radio wave field ($\omega = 2\pi f_{RF}$), the speed of light in vacuum, the dielectric permittivity of vacuum, and the magnetic permeability of vacuum. Heat generation due to radio wave dissipation is calculated according to,
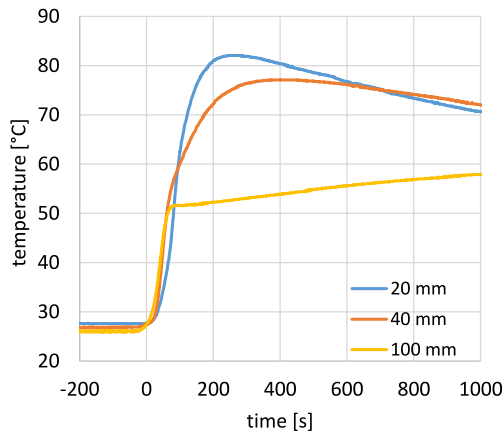
Fig. 2. Temperature recordings during field trial at different depths below soil surface (Sturm, et al., 2023; reprinted with permission). The time t = 0 is the instant at which the leading edge of the horn antenna crosses over the position of the sensors.

$$Q_{RF} = \frac{1}{2} \omega \varepsilon_0 \varepsilon'' \mathbf{E} \bullet \mathbf{E}^* \tag{14}$$

with ε'' being the imaginary part of the complex relative permittivity ($\varepsilon_r = \varepsilon' - i\varepsilon''$) of soil.

2.3. Pathogen model

The time and temperature dependence of pathogen inactivation is modeled with an Arrhenius expression,

$$N_L(t) = -\frac{k_{T_{ref}} \exp\left(\frac{E_a}{RT_{ref}}\right)}{\ln 10} \int_0^t \exp\left(-\frac{E_a}{RT(t)}\right) dt \tag{15}$$

The pathogen count varies over a wide range of orders of magnitude, therefore it is expressed in a logarithmic base (N_L, "L" for logarithm). The model parameters are: activation energy $E_a = 5.333 \cdot 10^5$ J/mol; reference rate $k_{T_{ref}} = 11.51$ 1/h; reference temperature $T_{ref} = 48.52$ °C, these kinetic parameters are derived from Pullman et al. (1981). The microorganisms that these parameters originate from are *R. solani*, *V. dahliae*, *P. ultimum*, and *T. basicola*. As explained in Section 1 this expression constitutes a basic model for biological effects that is primarily intended to provide a meaningful interpretation of the physical phenomena that occur during the radio wave treatment process. Refinement of the biology model would be a topic for subsequent studies. After the temperature transients in soil are calculated from the electromagnetic and transport equations in Comsol Multiphysics, they are exported into a Matlab environment. There the pathogen response is calculated according to the ordinary differential equation of Eq. (15).

2.4. Experimental data

As the model so far is a framework, it is too early to attempt simulation that closely approaches specific treatment cases. As discussed in the introductory section, there is insufficient information to establish model parameters, and in particular to define the biological processes that are at play. Moreover, at present there is limited experimental data to compare with.

Despite this state of affairs though, some comparison is desired to verify qualitative agreement between model and reality. To this end, two transient measurements are included here. These are measurements of temperature and pressure during two separate field trials.

The temperature transients (Fig. 2) are recorded with a set of Rugged Monitoring Lsens-U fiber optic temperature sensors. The sensors are
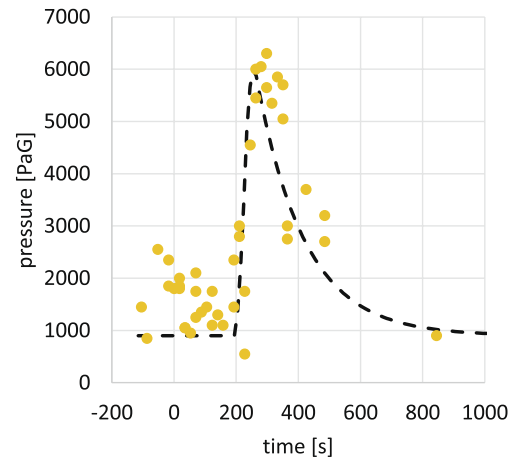

Fig. 3. Pressure recording during field trial, ~100 mm below soil surface (Sturm, et al., 2023; reprinted with permission). The time t = 0 is the instant at which the leading edge of the horn antenna crosses over the sensing tube position. The dashed line is included to guide the eye.

positioned at three depths with respect to the soil surface. The following observations can be made from these transients. Temperatures start to rise around the same time. This suggests that the radio wave field does not spread out much horizontally as it propagates through soil. As could be expected, the closer to the surface the measurement occurs, the higher the temperature is. There is a clear instant when heating stops for the transient at 100 mm depth at about 80 s, while the other two transients keep rising considerably. This rise is caused by heat transfer from the top 20 mm of soil where the highest temperatures occur that remained unrecorded in this test. The sensor at 100 mm also experiences a post-exposure temperature rise, but at a much lower rate. The two higher sensors reach their peak temperature around 250 s and subsequently cool down due to heat transfer to surroundings and to deeper soil layers. The 100 mm sensor keeps rising for the duration of the test, and ultimately reaches a temperature above the threshold temperature of 60 °C that was defined in our prior study to be the threshold for pathogen inactivation. For this particular test, the treatment depth would hence be at least 100 mm. This corresponds to field trials with pathogens in which a treatment depth of ~ 0.15–0.2 m has indeed been reached.

In contrast to the fiberoptic sensors that are compatible with radio wave exposure, the pressure sensor (SMC PSE543A) is kept out of the radiated electromagnetic field. Instead, a length of pneumatic tube of 6 mm outer diameter is positioned with its open end at a depth of around 10 cm in the soil under the path of the Agritron prototype. The other end is connected to the pressure sensor outside of the radio wave field. The pressure recordings (Fig. 3) exhibit fluctuations that are likely caused by pressure build-up and release in relation to deformation of soil. This is not modelled, therefore such behavior is not expected in the simulation. What the graph shows is that there is pressure development before the antenna reaches the position at which measurement occurs. Furthermore, there is a ~ 2 kPa pressure development initially, followed by sharp pressure peak to around 6 kPa. This peak occurs around 280 s, well after the antenna has passed the measurement position. From this, it would appear that the interaction between heat transfer, vapor pressure and flow can produce complex dynamics in the pressure transients with features such as delayed pressure peaks.

3. Methodology for simulation of steam treatment

The model is adapted to simulate the following configuration. A sheet is placed over the soil, steam is injected under this sheet, and porous vacuum pipes are placed in the soil to draw heat into the soil. The soil bed and the sheet have a standard width of 6.4, steam injection

occurs at every 10 m along the crop bed, the sheet expands to a height of 1 m. In accordance with practice, the sheet is thermally non-insulating, because insulation is commonly considered too heavy and too fragile to be applicable. Vacuum pipes are placed at a depth of 0.7 m at a mutual centerline distance of 1.6 m with a diameter of 80 mm and vacuum gauge pressure of 300 mbar. This corresponds to current practice, as described in personal communication with both JanityFlowers B.V. and MG GRAND B.V., both communications having occurred in 2020. Refer to Fig. 40 and Fig. 41 for a graphical representation of the configuration. Steam is supplied at a superheated temperature of 130 °C; under the sheet it is at ambient pressure. The treatment case considers steam generated by natural gas, applied for a period of 5 h, and a cumulative application of steam equivalent to 4 m^3 of natural gas per m^2 of soil.

Several alterations are made to the model. First, only the two-dimensional simulation step, and the step that calculates the pathogen inactivation are carried out. The three-dimensional simulation step that includes the antenna and electromagnetics is omitted, because these are not involved with the steam treatment case. Second, the boundary conditions at the top boundary of the soil volume (i.e. ground level) are adjusted to correspond to steam exposure. Third, in the geometry a semi-circle is positioned that corresponds to the vacuum pipes. Boundary conditions at the side of the soil domain constitute symmetry, so only half the pipe cross section is needed. On the boundary of this pipe the vacuum pressure is applied as boundary condition. Four, the flow of condensation water and heat transfer along with this flow are added to the model equations.

3.1. Boundary conditions at soil top surface for steam treatment

The boundary conditions at the ground level surface at which soil is in contact with steam are altered with respect to the radio frequency case in order to represent steam treatment. Appendix B details the derivation of the convection parameters. The resulting boundary conditions are outlined below.

Mixing in the steam volume under the sheet and heat transfer cause the temperature to drop well below the superheated temperature of the feed. At the steam/soil interface, a heat transfer coefficient of 71.56 W/m^{2}K with respect to steam at a temperature of 99.5 °C is imposed.

A similar convection model is employed to represent the transfer of water vapor between soil and steam. The heat of evaporation is adjusted though, because as steam condenses on the inside of the sheet, the associated heat of evaporation escapes to the ambient surroundings, while the condensation water that forms falls onto the soil. Hence the mass transfer coefficient accounts for the total of condensation water that forms with respect to saturated steam, while the heat of condensation is reduced to adjust for the heat lost through the sheet to surroundings. The resulting transfer coefficient for water vapor is 3.2 mm/s, and the adjusted heat of evaporation amounts to 1954 kJ/kg.

3.2. Flow of condensation water through soil

Steam is in intricate contact with soil once it enters into it, and the soil temperature cannot exceed the boiling point. It is therefore unlikely that steam remains in vapor phase once it enters into the soil. This has two consequences. First, all condensation occurs at the soil surface at or close to ground level, and all heat of condensation is released at that location. Second, the pressure difference with the vacuum pipes does not draw steam in vapor phase through the soil, but rather the hot condensation water. In addition to the vacuum suction, gravity also acts on condensation water, so this also needs to be accounted for.

These phenomena are represented by a flux vector for flow of liquid water through a porous medium according to Darcy's law,

$$\overline{u}_l = -\frac{k_l}{\mu_w \varphi_l}(\nabla p - \overline{g}\rho_w) \tag{16}$$

Electric field strength, logarithmic, log$_{10}$(E/1(V/m))
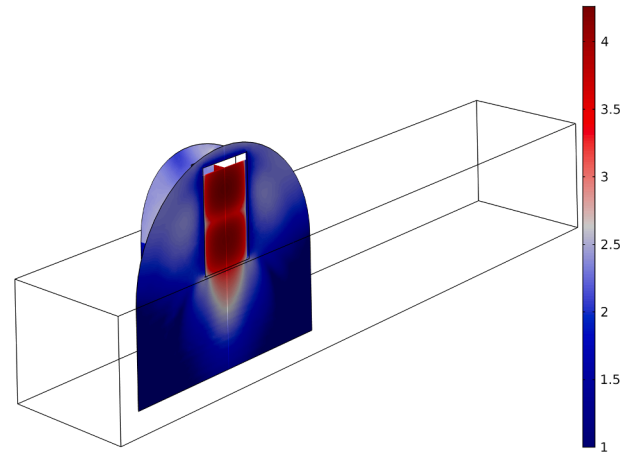
Fig. 4. Logarithm of the amplitude of the electric field vector component for the base case simulation.

Here $\overline{u}_l$ is the flow vector for liquid water through soil. The permeability term k_l is a function of n_{wl} (Bear, 1972). At the lowest value for n_{wl} the permeability k_l is zero, while at the level of saturation the permeability is increased to 10^{-6} cm^2, which corresponds to that of sand or gravel.

To describe the convective heat flux that is caused by this flow of liquid water, an additional term is introduced to Eq. (7),

$$\partial_t T_{sl}(\rho_s C_{p,s} + M_w C_{p,wl} n_{wl}) = \dots - M_w C_{p,wl} n_{wl}\overline{u}_l \bullet \nabla T_{sl} \tag{17}$$

The gradients on flow velocity and liquid water molar density are negligible relative to the temperature gradient. Therefore, only the contribution of latter to the heat balance is introduced here.

4. Base case simulation

The first part of the parametric study is to simulate a base case to compare parametric variations against. This base case simulates a net radio wave power of 50 kW through the complete antenna, which corresponds to 25 kW through the half of the antenna that is included in the simulated geometry. An antenna travel velocity of 6 mm/s is imposed. Soil humidity is 20 m%, and porosity is 5 %, Darcy permeability is 10^{-9} cm^2. The conductivity contribution to the dissipative properties of soil is expressed in terms of a dry mass equivalent of NaCl present in soil. The exact ionic soil composition and its influence on electromagnetic medium properties are beyond the scope of this present work, this simplified equivalent description is therefore employed. The salinity is set to 0.06 dm% of NaCl equivalent. The initial soil temperature is 10 °C, and the temperature of ambient air is 20 °C at a relative humidity of 40 %. At the initial conditions, this results in a dielectric permittivity of 17.78 – 4.68i, a thermal conductivity of 2.1 W/mK, and a diffusivity of liquid water in soil of 5.4·10^{-8} m^2/s.

The resulting simulated electric field amplitude (Fig. 4, logarithmic scale) exhibits a main emission lobe that is directed downwards into the soil. A zone of heat generation occurs directly under the antenna (Fig. 5). It stretches over the width of the antenna and to a depth of about 0.2 m. Emission lobes are also present above the soil surface. These constitute an emission loss to surroundings.

It has to be noted that the particular antenna configuration that is simulated has no design features that shield emission to the surroundings, nor does it have any impedance matching to limit reflection loss. *In contrast, the Agritron prototype depicted in Fig. 1 does have such features and has been verified to have sufficient suppression of emission and reflection losses.* Specifically, the absence of excessive emission losses was verified with both a ETS-Lindgren HI-1600 survey meter and the combination of
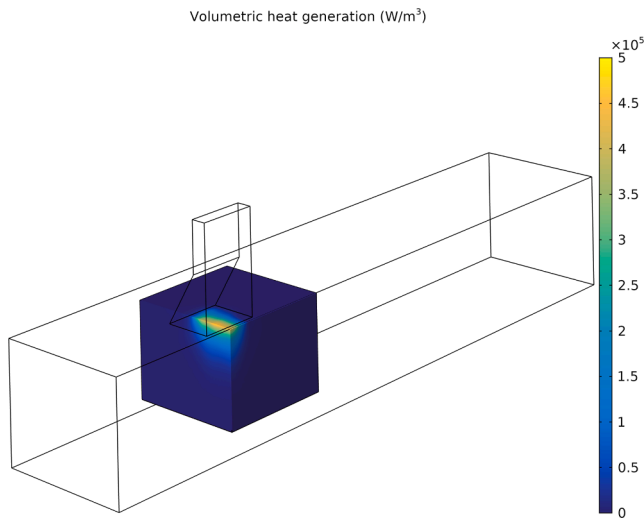
Volumetric heat generation (W/m^3)

Fig. 5. Base case volumetric heat generation due to radio wave heating.

Pressure difference (Pa)
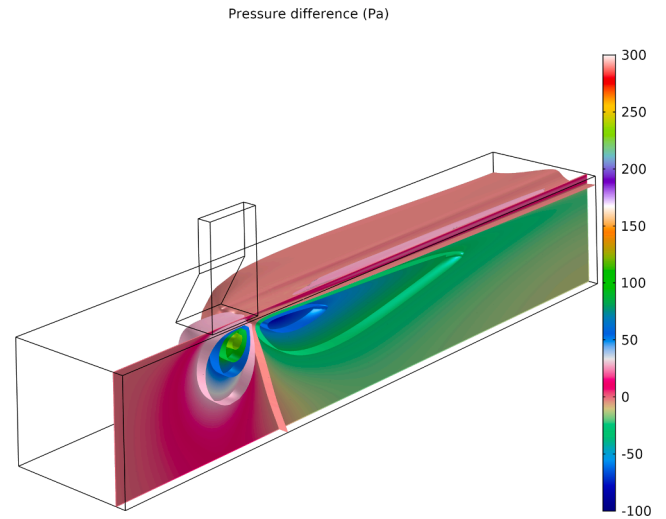
Fig. 7. Pressure variations in soil for the base case.
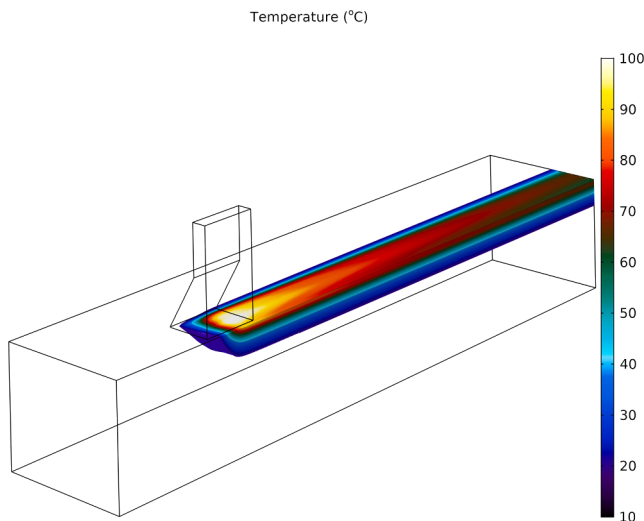
Temperature (°C)

Fig. 6. Simulated temperature for the base case.
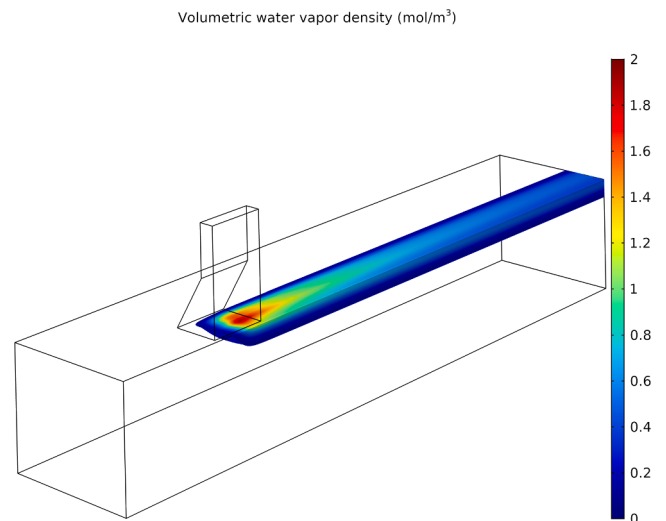
Volumetric water vapor density (mol/m^3)

Fig. 8. Water vapor density, base case.

a Siglent SVA1015X spectrum and vector network analyzer and a Tex-box TBPS01 probe kit. Moreover, the reflection losses of the Agritron prototype are managed with the built-in reflected power measurement of the 100 kW 915 MHz generator and stub-impedance tuner (all elements of the 915 MHz circuit by Sairem). The design features that enable suppression of radio wave losses are not subject of this present research, and are therefore not included in the model geometry (Figs. 4-9). In lieu of simulated suppression of losses, in the simulation the power output is scaled to provide the desired amount of heating in the soil, which is a sufficient functional resemblance of suppression of losses for the purposes of this study.

The heat that is generated results in a track of increased temperature in the soil (Fig. 6). This increases vapor pressure in the soil, which results in a pressure response (Fig. 7) that stretches well beyond the zone in which temperature effects occur. The pressure pattern is not unlike a bow wave, with an initial pressure increase followed by a subsequent pressure drop once temperature gradually falls after exposure. The pressure dynamics vary considerably with the process parameters though, as will be shown in Section 5 below.

The response of molar vapor density (Fig. 8) is closely correlated to that of temperature, which is to be expected because the partial vapor density is a function of temperature. In contrast, the liquid water density (Fig. 9) drops only gradually after heating, and only in a shallow top

layer of soil. Humidity drops due to evaporation, which is restricted by the rate at which water is able to evaporate to the ambient surroundings. At the soil surface this occurs gradually for as long as there is a raised temperature to drive evaporation, while in deeper soil layers evaporation to surroundings is limited by transport through soil.

In addition to the three-dimensional color mapped slice graphs, a number of line graphs are presented here too in order to visualize particular process aspects in closer detail.

Temperature transients over long and short time intervals (Fig. 10 and Fig. 11) show an initial rapid temperature rise during radio wave exposure followed by much slower temperature redistribution. The closer to the soil surface, the higher the temperatures are, because the electromagnetic field decays as it travels deeper into the soil. This is also apparent in an instantaneous vertical distribution profile for heat generation (Fig. 12), which decays to zero as the depth increases. The distribution along the direction of antenna travel (Fig. 13) resembles a plain bell curve. The magnitude of heat generation varies with depth, but the shape of the respective depth curves is invariant. The heating rate distribution across the direction of travel (Fig. 14) however is more complex, which relates to the specific antenna design. The intensity of heating to the side is higher than it is in the middle, which could possibly turn out to be beneficial in this specific case. Over time, the temperature
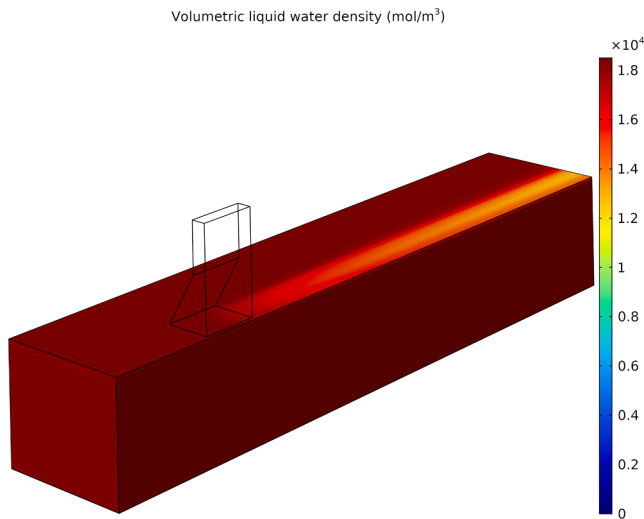
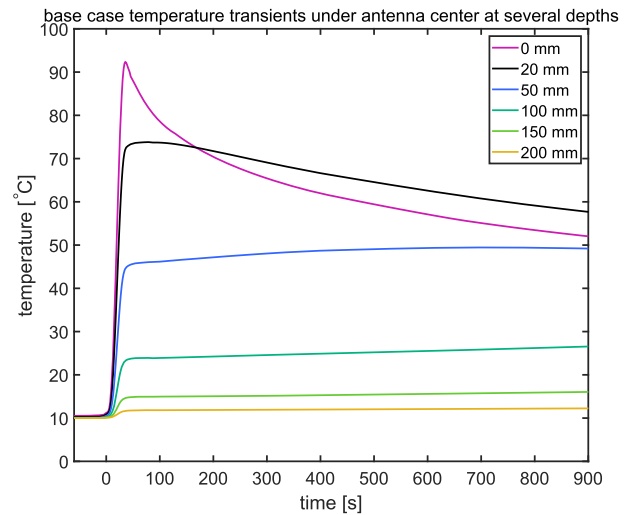**Fig. 9.** Liquid water density, base case.

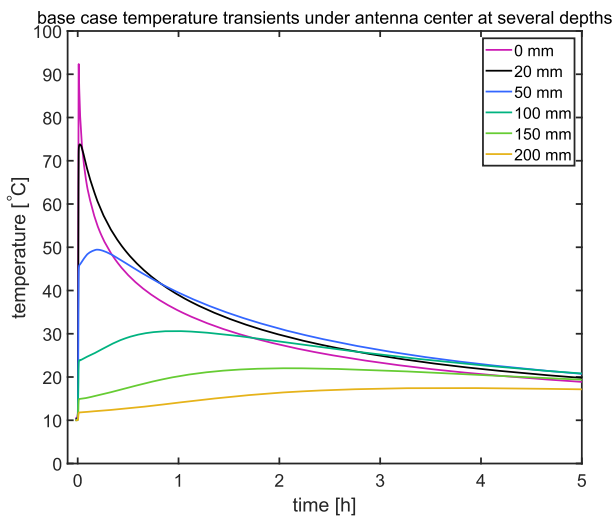**Fig. 11.** Simulated temperature transients over a 15 min period.

Fig. 10. Simulated temperature transients over a 5 h period.
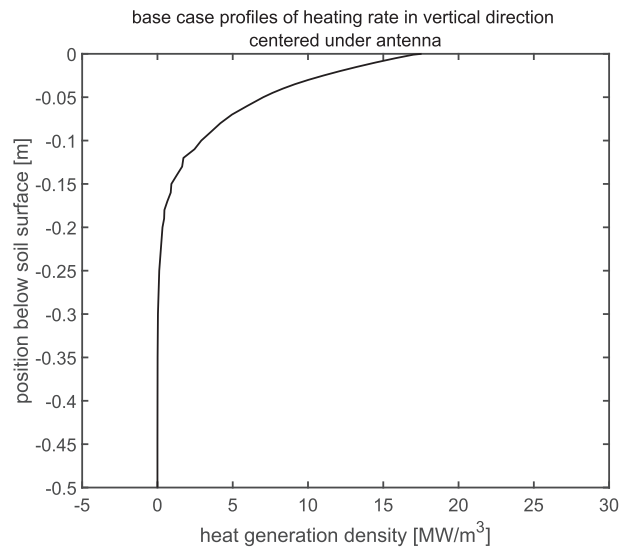

Fig. 12. Vertical heating rate distribution below the antenna center.

development redistributes such that an even temperature profile results over the width of the antenna (Fig. 15). This in turn translates into a fairly even distribution of the treatment effectiveness, as is shown in the 99.9 % pathogen inactivation contours (Fig. 16). In addition, it can be seen that the treatment process is fairly rapid; after only two minutes the final treatment contour of 99.9 % is already closely approximated.

As was calculated in our prior study, for this particular simple pathogen model at these short treatment times, pathogen inactivation occurs at a temperature threshold of around 60 °C. The 99.9 % inactivation contours are shown here, but contours for inactivation to lower orders of magnitude lie close to the 99.9 % ones that are shown in Fig. 16. How the short treatment time would affect realistic and more complex biological processes would be a tenable subject for subsequent investigation. Another remark that needs to be made here, is that a distinction needs to be made between on the one hand the treatment depth that is defined by these contours, and on the other the penetration depth for electromagnetic propagation that depend on by the effective dielectric medium properties and the frequency. The latter is characterized by the rate of decay along the direction of propagation of the electromagnetic energy flux, while the former is defined by the depth at which the temperature reaches the temperature threshold. To illustrate the difference, consider two cases: one in which a very low radio wave power is applied; and one in which a high power is applied, with all

other parameters being the same. For both cases the penetration depth is identical, but the treatment depth is different. For the low power case, the temperature may not have reached the temperature threshold an any place, which results in a zero depth of treatment. In contrast, for the high power case, the threshold can be reached at a depth that exceeds the penetration depth.

The pressure transients (Fig. 17) show the earliest pressure response precede the temperature response. The maximum pressure peak concurs with the maximum heating rate and the maximum rate of evaporation. After the antenna has passed, temperature starts to fall gradually in the higher soil layers, which causes the vapor pressure to drop and a vacuum to form.

Fig. 18 shows vertical humidity profiles of the soil after two minutes, fifteen minutes and one hour. It shows more clearly than Fig. 9 how shallow and slow acting the effect on the moisture content of soil is. This is a useful observation for subsequent numerical simulation studies, because it suggests that humidity variation does not greatly affect the dielectric properties of soil at the moment at which the antenna is overhead. The moisture content response is therefore not likely to influence the electromagnetic interactions in soil, which could possibly allow for a simplification of the simulation approach by avoiding the bidirectional coupling between electromagnetics and the transport of
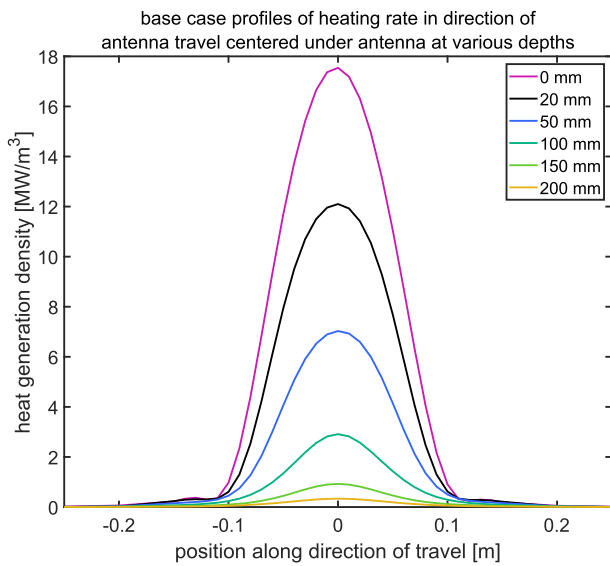
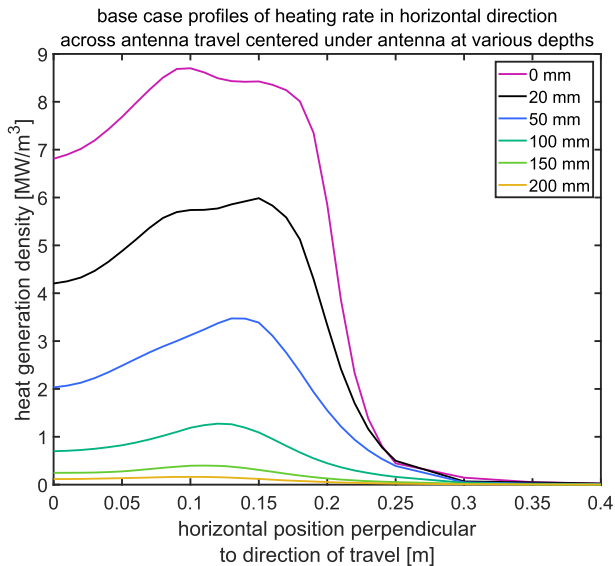**Fig. 13.** Heating rate distribution along direction of antenna travel.

Fig. 14. Heating rate distribution across direction of antenna travel.

Fig. 15. Temperature contours.

Fig. 16. Pathogen inactivation contours.

moisture.

5. Parametric study for individual parameters

A systematic parametric study is performed in order to investigate how the individual physical parameters influence the treatment process. In this study, parametric variations with respect to the base case are applied. Below, the cases of parametric variation are outlined. This is followed by eight sub-sections that discuss the effect of variation of the individual parameters.

The primary motivation is to use the insight that is gained to develop the treatment process. In addition though, there is also the desire to understand the phenomena that are observed experimentally. As can be observed, the experimental transients presented in Section 2.4 are dissimilar from the base case simulation that is presented in Section 4. At this stage of model development, it is not yet expected to have a quantified agreement between experiment and simulation. Nevertheless, simulations can help to understand qualitatively the experimental observations. Hence, the simulation result presented in this section are in a
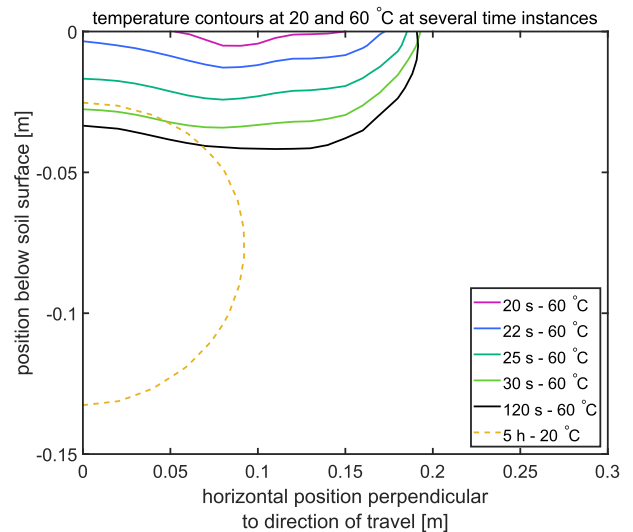
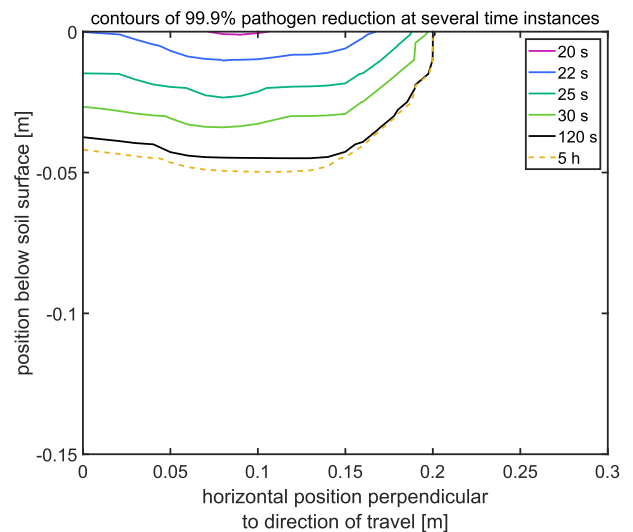select number of instances used to interpret those observations.

A total of eight physical and processing parameters have been explored via simulation of parametric variations with respect to the base case. These are outlined as follows:

1. Soil porosity, or the relative volume occupied by gas and vapor in the soil. The base case porosity is 5 vol%, this is varied to 2.5, 10 and 20 vol%.
2. The duration of pre-drying. Specifically, the duration of the period in which the soil of initially homogeneous humidity and temperature (20 m%, 10 °C) is dried by being exposed to ambient air (relative humidity of 40 %, 20 °C) prior to radio wave treatment. This causes the top layer of soil to have a reduced humidity during this treatment. These drying periods are 120, 240 and 360 h respectively.
3. Soil salinity. The base case has 0.06 dm% NaCl equivalent, while parametric variations of 0.03, 0.09 and 0.12 dm% are applied.
4. In addition to soil humidity variations due to pre-drying, also homogeneous variation of the initial soil humidity is explored. The base case has a humidity of 20 m%, and this is varied to 5, 10 and 30 m%.
5. The Darcy permeability that describes gas and vapor transport may vary over multiple orders of magnitude over the range of various
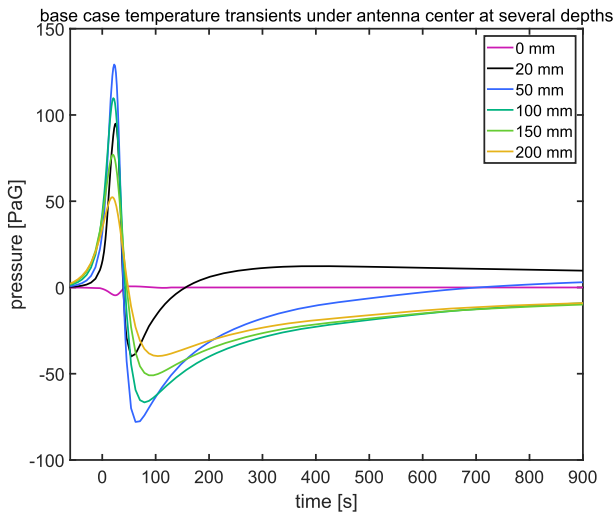
Fig. 17. Pressure transients of the base case. The transients show pressure difference with respect to the ambient pressure.
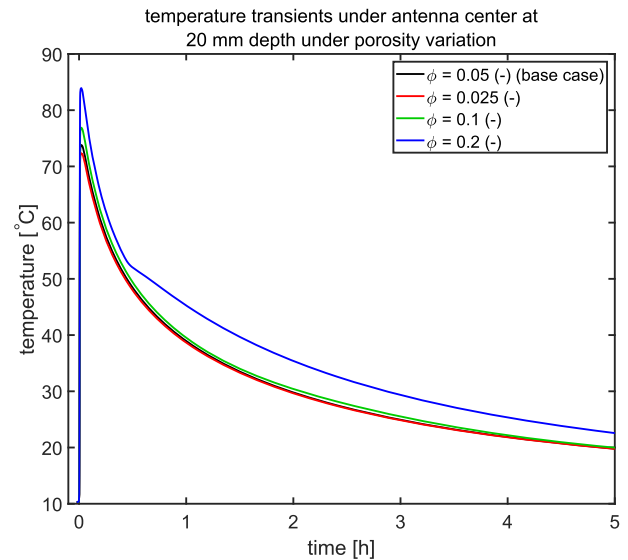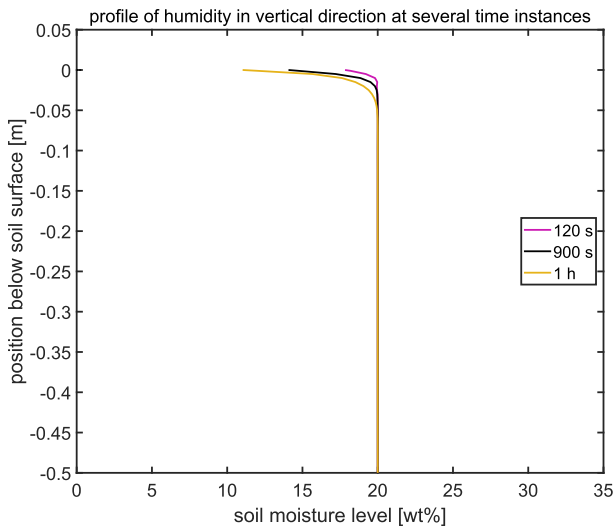

Fig. 18. Vertical humidity profiles.

relevant soil types (Bear, 1972). Consequently, the range of variations that are considered herein are equally wide: the base case has a permeability of 10^{-9} cm^2, and the parametric variations comprise of 10^{-5}, 10^{-7} and 10^{-11} cm^2.

6. Thermal conductivity of soil. The thermal conductivity of soil is not defined as a singular constant parameter value. Rather, it depends on soil humidity, which is a variable that may change in the simulation. Therefore scale factors are applied to the thermal conductivity in order to alter it. For the base case this factor is 1, and for the parametric variations simulated herein it is 0.5, 1.7 and 2.5.

7. Coordinated variation of velocity and radio wave power. In the context of demand response applications, when radio wave power is dictated by external factors such as fluctuating availability of renewable resources, it would be relevant to evaluate operation where the antenna speed is adjusted to match the available radio wave power. The speed would then be adjusted to maintain a constant energy applied per unit of distance traveled. The base case has a velocity of 6 mm/s and radio wave power of 50 kW, while the parametric variations that are considered are 3 mm/s and 25 kW, 4 mm/s and 33.33 kW, and 10 mm/s and 83.33 kW.

8. Variation of radio wave power while maintaining the same 6 mm/s antenna velocity, which alters the application of radio wave energy

Fig. 19. Temperature transients under porosity variation.

per unit antenna travel distance. The base case has a power of 50 kW, the parametric variations considered are 25, 33.33 and 83.33 kW.

5.1. Porosity variation

As porosity increases, two effects occur; first, the volumetric heat capacity of soil decreases because less soil and moisture are present per unit volume; second, the diffusivity of pressure decreases. Due to the former effect, there is a larger short term temperature increase as porosity increases (Fig. 19). The latter effect causes larger and more sharply defined pressure variations to occur (Fig. 20). As with the graph of experimental pressure recordings (Fig. 3), the simulated pressure transients exhibit pressure peaks with delayed onset. In particular the $\varphi = 0.2$ curve has a pressure rise approximately half an hour after radio wave exposure. Close inspection of the simulation results showed that zones of high pressure migrate through the soil. As these zones reach the position at which the transient is recorded, a pressure rise occurs. These zones take along with them zones of increased vapor pressure, which is coupled to the local temperature. Consequently, the temperature transient for $\varphi = 0.2$ exhibits a relatively sharp bend at the time instance at which the aforementioned pressure peak occurs. At that instance, the increased vapor pressure reduces the volumetric rate of evaporation and lowers the extraction of heat of evaporation, which results in lower a lower rate of temperature decrease. As for the pathogen suppression, increased porosity enables higher temperatures, and therefore a better treatment depth (Fig. 21).

5.2. Variation of the duration of pre-drying

Pre-drying the top layer of soil to the surroundings could be a useful method for soil preparation prior to radio wave treatment. It will reduce the electromagnetically dissipative properties of soil, which causes less radio wave energy to be converted into heat in these higher soil layers, and leave more of this energy to propagate deeper into the soil. In principle, this could allow for a deeper treatment effect. In addition, a lower humidity will reduce the thermal mass of the top layers of soil, which reduces the energy requirement to achieve a threshold temperature.

As demonstrated in Section 4, transport of moisture in soil occurs over relatively long time scales. Consequently, pre-drying is applied over a time scale of weeks in the simulation: 120 h, 240 h, resp. 360 h. The resulting simulations show that the humidity reduction due to pre-
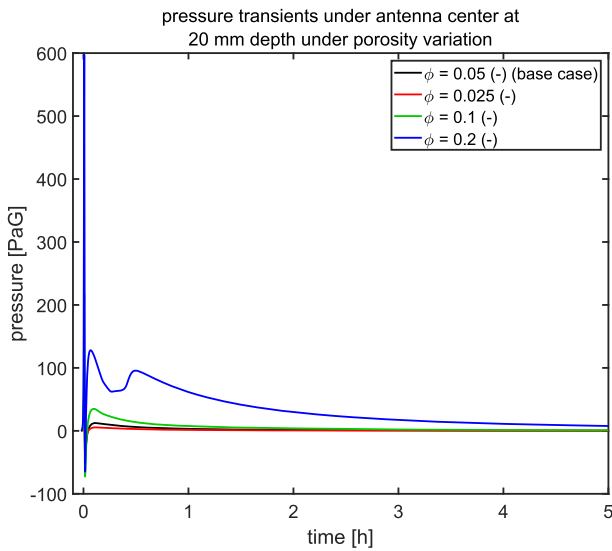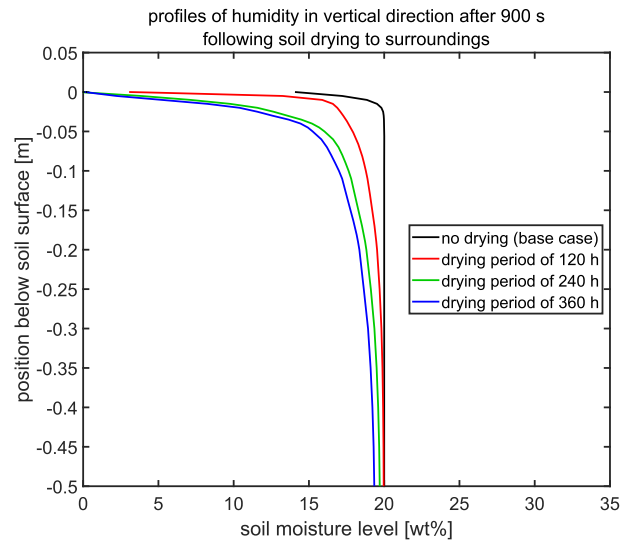
pressure transients under antenna center at 20 mm depth under porosity variation

Fig. 20. Pressure transients under porosity variation.

contours of 99.9% pathogen reduction after 120 s under porosity variation

Fig. 21. Pathogen inactivation contours under porosity variation.

profiles of humidity in vertical direction after 900 s following soil drying to surroundings

Fig. 22. Vertical humidity profiles shortly after radio wave exposure for cases with different pre-drying duration.

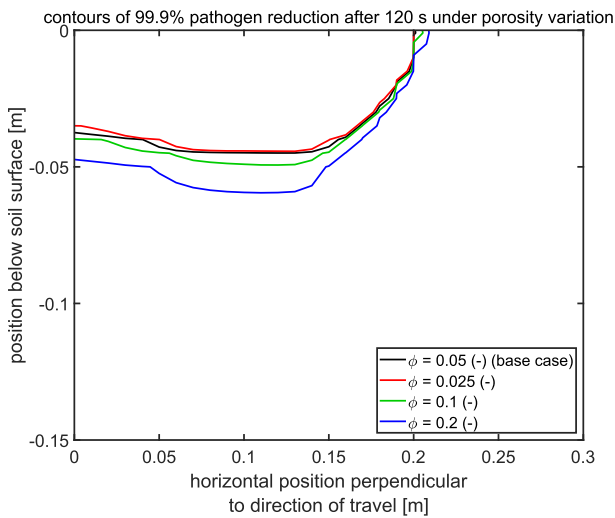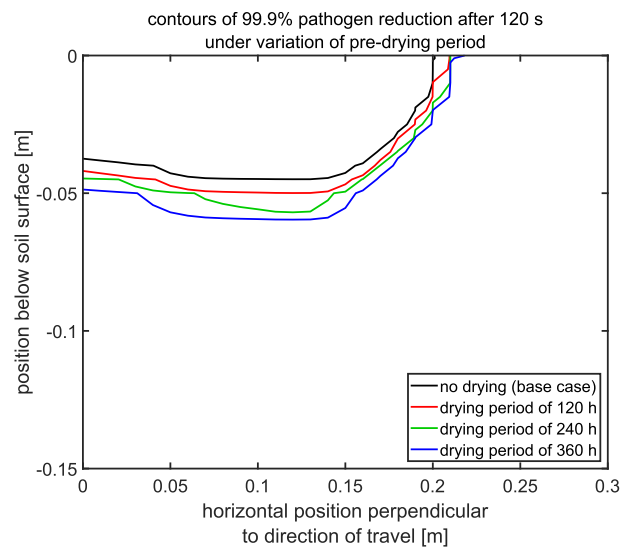## contours of 99.9% pathogen reduction after 120 s under variation of pre-drying period

Fig. 23. Pathogen inactivation contours for pre-drying duration variation.

drying is much more extensive than the effect of radio wave exposure (Fig. 22). The pathogen inactivation curves (Fig. 23) confirm that a deeper treatment effect is achieved in case soil is left to dry to air over extended periods of time. Due to the thermal mass effect, the temperatures in the top soil layers are higher despite the reduced heat generation at these locations. This results in increased vapor pressure as well as increased pressure. Hence, the pressure transients reach much higher peak values as soil has been left to dry for longer (Fig. 24). In addition, the vacuum effect that could be observed in the base case no longer occurs. The three-dimensional distribution affirms this observation; the pressure distribution is completely different from the base case (Fig. 25 vs. Fig. 7), and a vacuum no longer occurs for pre-dried soil. Although the peak pressure variations in these simulations do not yet approximate the experimentally recorded peak pressure (Fig. 3), they suggest that surface dryness during such tests can likely have a significant effect on the pressure development.

5.3. Soil salinity variation

The dissipative properties of soil are altered by varying the soil salinity. Expressed in NaCl-equivalent, it is changed to 0.03, 0.09 and 0.12 dm%, with a base case value of 0.06 dm%. Since it is closely correlated to the dissipative properties, the salinity effects are apparent in the vertical distribution of heat generation in soil (Fig. 26). Higher salinity increases the loss factor, which causes more electromagnetic energy to be dissipated in the vicinity of the soil surface. For deeper soil layers however, less energy remains to be dissipated there. Therefore, for higher salinity, the heat generation is higher near the surface, but decays more rapidly with depth. There is cross-over point at a depth of around 5 cm below which increased salinity causes less heat generation. Consequently, there is no straightforward monotonic relation between the treatment depth and salinity. In case the initial treatment depth is below the cross-over point, increasing salinity will reduce treatment depth, as more radio wave energy will be dissipated closer to the surface and less remains for deeper layers. In contrast, if the effective treatment depth is initially above the cross-over point, then the reverse will occur, and higher salinity causes a deeper treatment. For the particular cases in this study though, the treatment depth is close to the cross-over point and no significant effect on pathogen inactivation occurs.
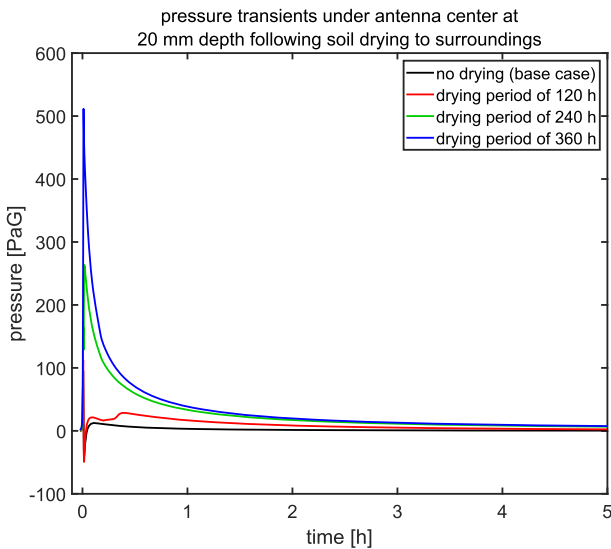
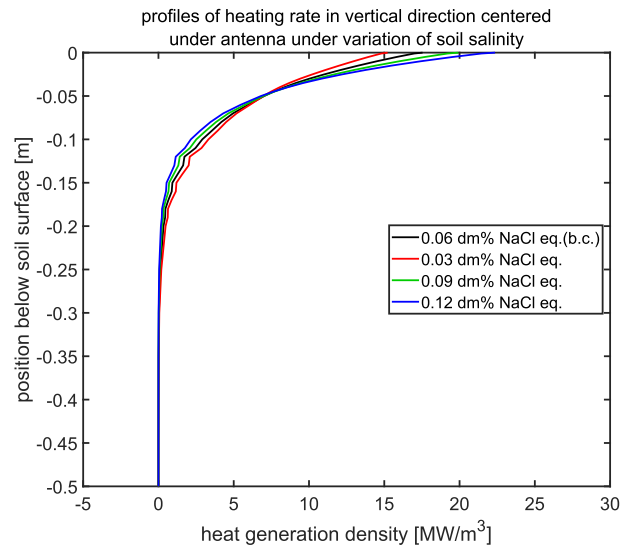**Fig. 24.** Pressure transients for pre-drying duration variation.

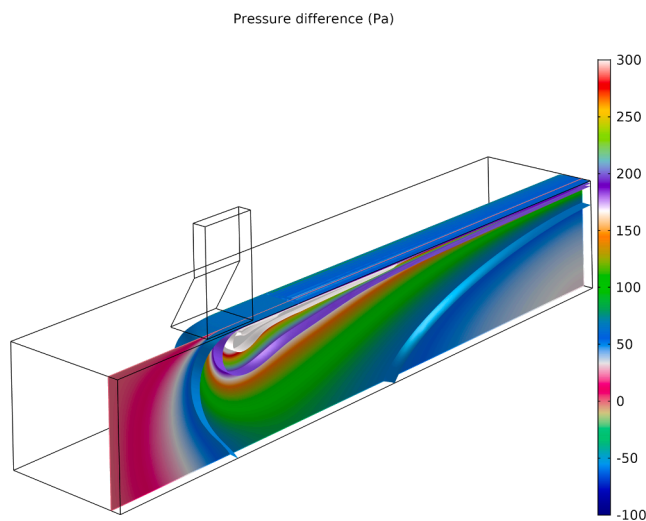**Fig. 26.** Vertical heat generation profiles under salinity variation.

Fig. 25. Distribution of pressure variation in soil for the case of 360 h pre-drying.

Fig. 27. Pathogen inactivation contours under homogeneous soil humidity variation.

5.4. Soil humidity variation

In the set of simulations discussed in Section 5.2, the top layers of soil are left to dry to ambient air prior to radio wave exposure. This causes a heterogeneous humidity distribution with a lower humidity near the surface. This is supplemented here by a simulation of homogeneous variation of soil humidity prior to treatment. Humidity has a similar effect as salinity has; increased humidity results in a higher dielectric loss factor. This causes more dissipation to occur for a particular radio wave field strength, and a more rapid decay of this field strength as a radio wave field travels through soil. In addition, increased humidity increases the thermal mass of soil, which reduces temperature for a particular amount of dissipated radio wave energy. The net effect in this particular case is that lower humidity results in slightly shallower treatment (Fig. 27). Nevertheless, the reverse may also occur, depending on the particular case. The crossover phenomenon described in Section 5.3 in the context of salinity variation also occurs with humidity variation. In addition, these simulations also exhibit the characteristics of shifting high pressure zones. The 5 m% and 10 m% temperature transients show sharp bends in the temperature curves (Fig. 28) that
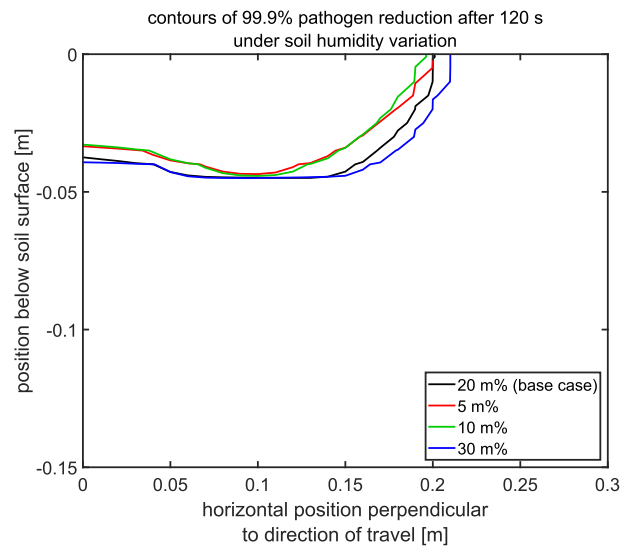
concur with a rapid increase in pressure (Fig. 29). Clear patterns could not be found that may predict these phenomena.

5.5. Darcy permeability variation

Variation of the Darcy permeability has negligible temperature effect. All temperature transients effectively are overlays of the base case temperature (no graphs included herein). Moreover, the 60 °C temperature contours and pathogen inactivation contours are also the same as for the base case. The only notable difference can be found in the pressure response. The pressure transients under variation of permeability show much larger pressures effects for smaller permeability (Fig. 30). It would appear that the pressure variations are inversely proportional to the Darcy permeability. Since the Darcy permeability may vary over orders of magnitude, this could be another relevant factor in relation to the high pressure that was observed experimentally (Section 2.4, Fig. 3), but could not be initially observed in the base case simulation (Fig. 7, Fig. 17). Under variation of Darcy permeability there is better agreement. Specifically, the 10^{-11} cm^2 curve compares quite well to the experimental data with a peak pressure of similar magnitude.
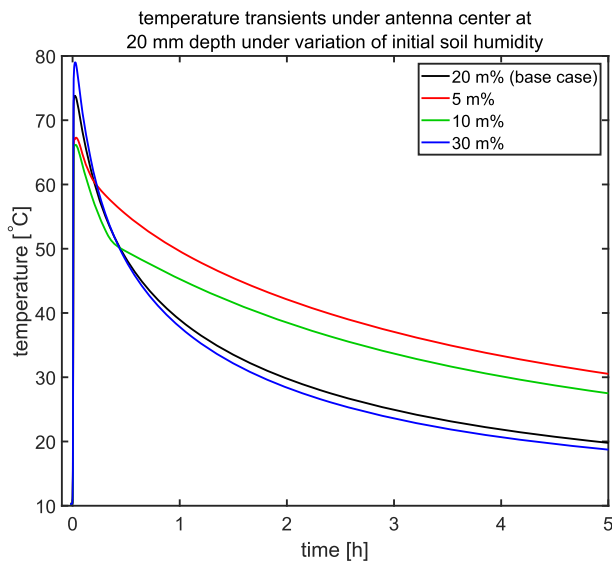
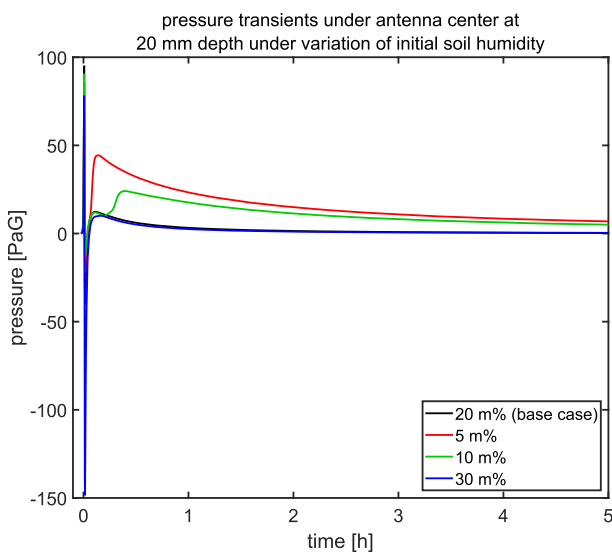**Fig. 28.** Temperature transients under homogeneous humidity variation.

Fig. 29. Pressure transients under humidity variation.

Fig. 30. Pressure transients under permeability variation.

Fig. 31. Temperature transients under coordinated power and velocity variation.

5.6. Thermal conductivity variation

Variation of thermal conductivity only affects heat transfer and temperature distribution over longer time periods. For the base case simulation as well as for the simulations of the parametric variation of thermal conductivity, the treatment effectiveness is determined exclusively in the first few minutes after radio wave exposure. Longer term physical phenomena like heat transfer have little effect on the treatment effectiveness. As with variation of Darcy permeability, variation of thermal conductivity has little effect on treatment effectiveness (no graph included). Section 6 examines if this also holds for a case in which a larger amount of energy is introduced into the soil.

5.7. Coordinated antenna velocity and power variation

Adjusting radio wave power and antenna speed to the availability of a renewable power source is a relevant consideration with respect to changes in energy markets. To investigate this type of operation, three treatment settings are simulated with respect to the base case, with proportional variation of antenna velocity and radio wave power. There
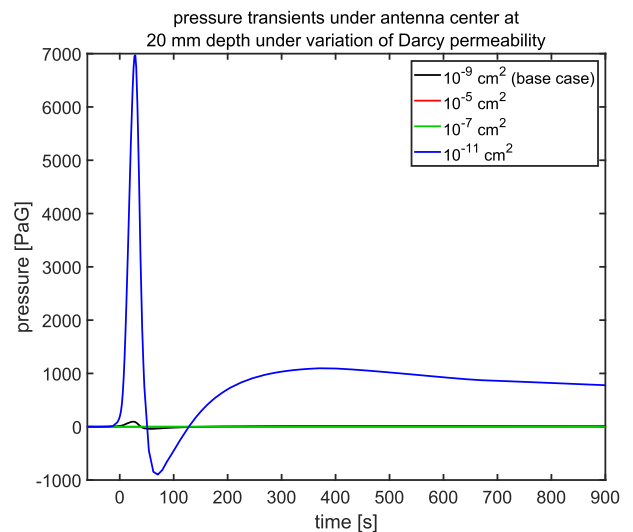
are differences in the resulting transients between these cases, but these occur over short time scales, as shown by the temperature and pressure transients (Fig. 31, Fig. 32). For higher velocity, the initial temperature rise is sharper, and the pressure variations are compressed, i.e. occurring over shorter time spans and with higher magnitudes. Pathogen inactivation is essentially the same between these cases though (Fig. 33). This confirms that radio wave treatment indeed may have sufficient flexibility to accommodate a fluctuating renewable power source, and that it could in principle be effective as a demand response application.

5.8. Radio wave power variation

The main process variable that determines the treatment effectiveness is the radio wave energy deposited per unit antenna travel distance. To explore this parameter four simulations with varying radio wave power at equal antenna velocity are performed. As could be expected, temperature (Fig. 34) and pressure (Fig. 35) variations are higher with increased power. For the highest power of 83.33 kW, the temperature actually rises above the boiling point of water. In that case the soil has completely dried out at the surface. The pressure is much higher for the
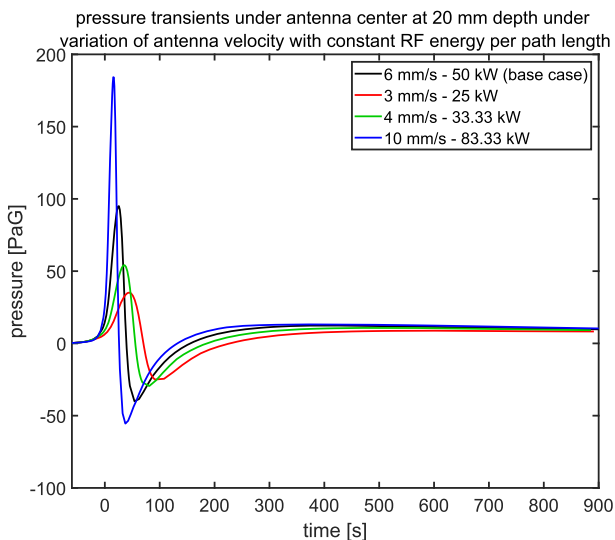
Fig. 32. Pressure transients under coordinated power and velocity variation.
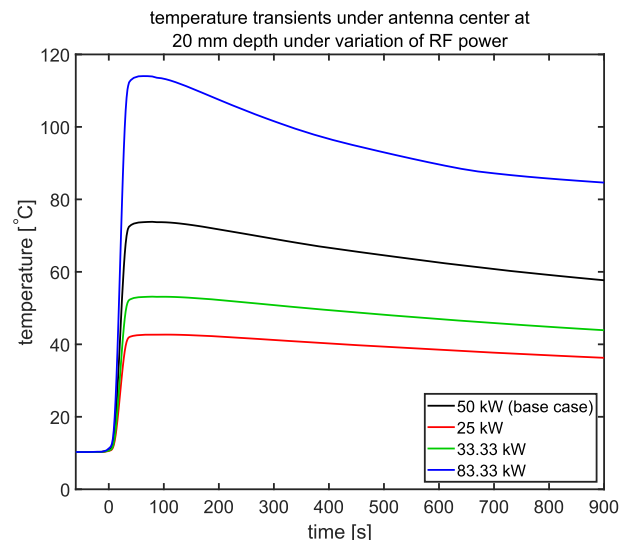

Fig. 34. Temperature transients under power variation.
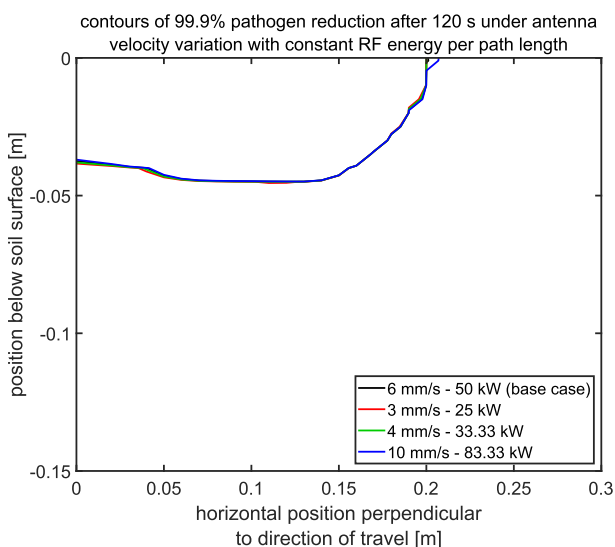

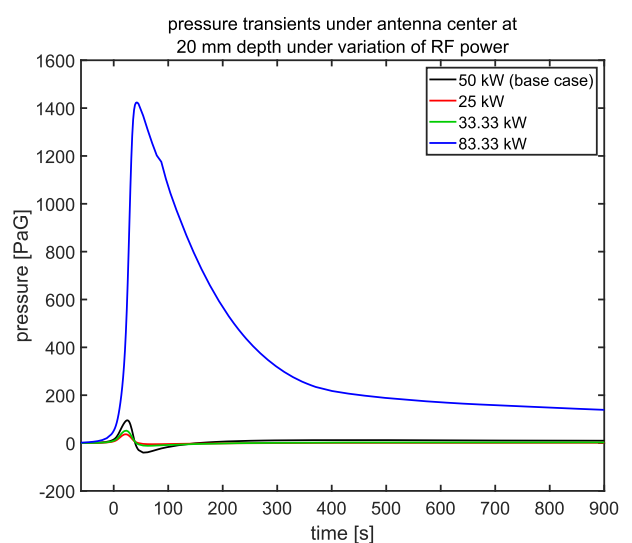Fig. 33. Pathogen inactivation contours under coordinated power and velocity variation.

Fig. 35. Pressure transients under power variation.

83.33 kW case then for the other cases, and forms one single pulse with a tail in the order of minutes. This is also reflected by the morphology of the pressure distribution (Fig. 36): there is a single pulse and subsequent decay without the formation of a vacuum. Despite the fact that 83.33 kW simulation involves only 66 % more radio wave energy, the pressure effect is disproportionately larger because of the non-linear relation between temperature and vapor pressure. The magnitude and duration of pressure effects have a degree of similarity to the experimentally observed transient (Fig. 3), though the pressure pulse delay of several minutes does not occur in the simulation.

At the lowest power of 25 kW, temperature does not even reach the 60 °C threshold. Hence, at this power no effective treatment takes place as is shown by the pathogen inactivation contours (Fig. 37). For the other power levels, there is an appreciable pathogen effect, and the treatment depth appears by approximation proportional to the radio wave power.

6. Simulations to verify replication of physical trial

As was clarified in the introductory section, a knowledge base on the exact physical and biological parameters is yet to be developed. Consequently, the base case simulation was not a-priory expected to replicate the performance that was observed during field trials. In this present section, a set of supplementary simulations are discussed that verify whether the simulation is able to yield a treatment effectiveness similar to those observed experimentally. This would amount to a treatment depth of around 0.15–0.20 m, though this figure could be subject to optimization of the treatment process and/or further development of the treatment system, so a deeper treatment effectiveness cannot be ruled out at this point.

For this verification, an additional simulation is performed in which parametric variations are applied that are expected to yield a deeper treatment. The specific parameters are outlined as follows. The surface porosity is 20 % and reduces gradually to 5 % at a depth of 0.15 m at which it remains for deeper depths. This resembles the physical case in which the top soil layer is loosened, while lower layers are compressed by the weight of the higher layers. The nominal humidity of soil is set at 7 m%, but a pre-drying period of 360 h is applied to reduce the humidity of the top soil layer. At the surface this reduces the humidity to 1 m%, which gradually increases with depth to the bulk humidity over a distance of 0.1 m. An antenna velocity of 3 mm/s and a net radio wave
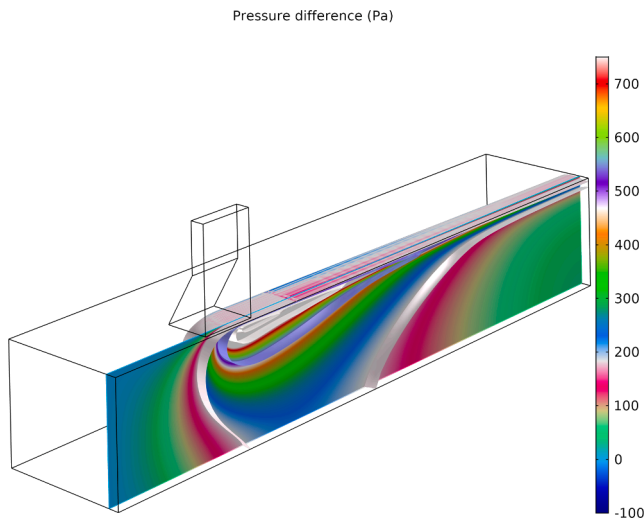
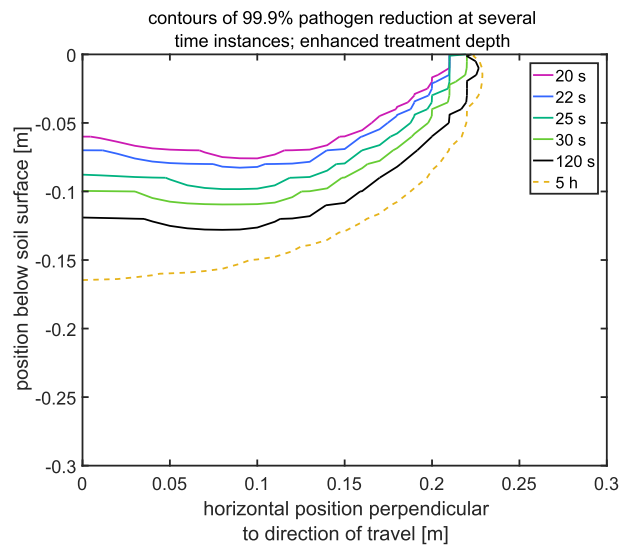**Fig. 36.** Distribution of pressure variation in soil for the 83.33 kW case.

Fig. 37. Pathogen inactivation contours under power variation.

Fig. 38. Pathogen inactivation contours under enhanced treatment depth (note the different vertical scale with respect to prior figures).
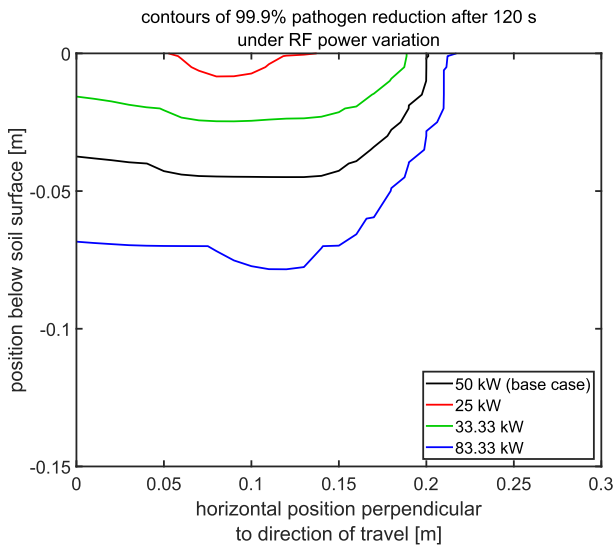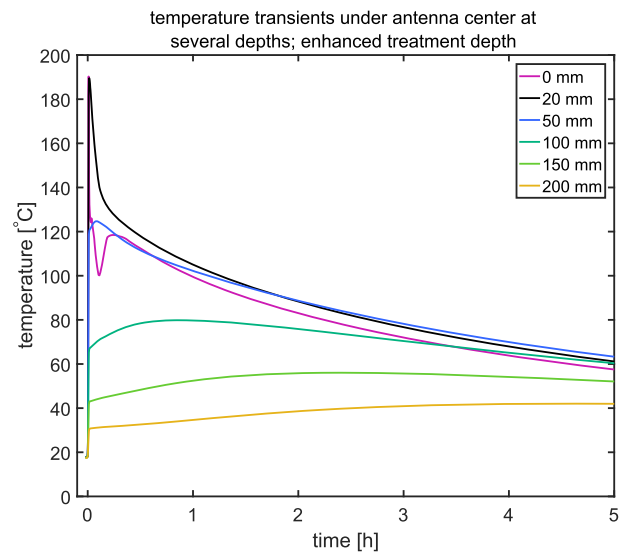

Fig. 39. Temperature transients under enhanced treatment depth.

power of 83.33 kW are applied.

The resulting pathogen inactivation contours (Fig. 38) present a treatment depth that has increased to around 0.15 m, roughly three times as deep as the base case. Also in contrast to the base case simulation, this simulation with enhanced treatment depth has considerable progression of treatment over longer time periods. The treatment effect is no longer settled in the first minutes after radio wave application; instead there is significant heat transfer downward post-exposure. This causes the ultimate treatment depth to be reached over the course of hours following radio wave exposure, although the majority of the treatment effect still occurs in the first minutes.

The cause of this delayed effect is the relatively large excess of heat that is introduced into the soil. The temperature transients (Fig. 39) for the enhanced depth simulation present much higher temperature values than in prior simulations. After moisture has evaporated, the boiling point of water no longer poses an upper limit on temperature. Therefore, in proximity to the antenna, the temperatures rise to higher values. The excess heat in higher layers then diffuses deeper into the soil with time, which results in additional pathogen inactivation. Further supplementary simulations are performed with increased thermal conductivity and increased Darcy permeability in order to evaluate the effect of increased diffusivity of the associated transport phenomena. It turned out that an

increased thermal conductivity results in more rapid spreading of thermal energy throughout soil, though neither parametric variation ultimately affects the treatment depth to a significant degree. Earlier observations in Section 5 with respect to the invariability of the treatment depth under variation of transport properties still hold for the cases of enhanced treatment depth. Finally, it is confirmed that a treatment depth in accordance with experimental observations is reproducible in simulation.

7. Simulation of steam treatment

Simulated temperature fields after 5 and 12 h of steam treatment (Fig. 40 resp. Fig. 41) show that the temperature effects reach much deeper than for radio wave treatment. These results also show that the steam treatment process takes much longer. This is further illustrated by the temperature transients at 20 mm depth (Fig. 42) for both treatment methods. The radio wave case reaches the threshold temperature in minutes, and subsequently cools down over the course of a number of hours. In contrast the transient for steam treatment reaches the 60 °C threshold in about half an hour. The pathogen inactivation contours
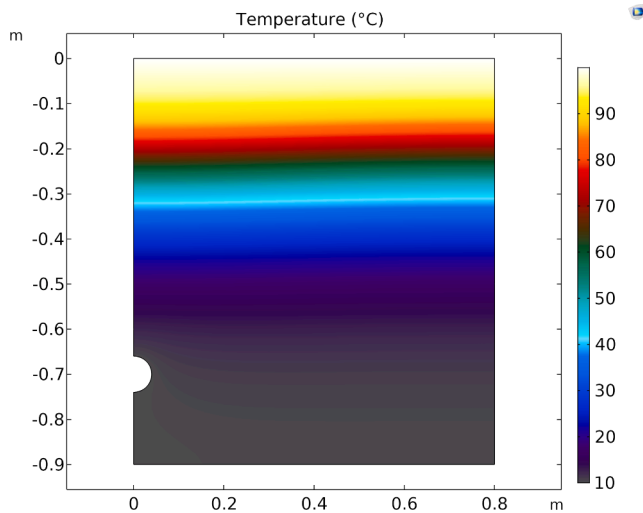
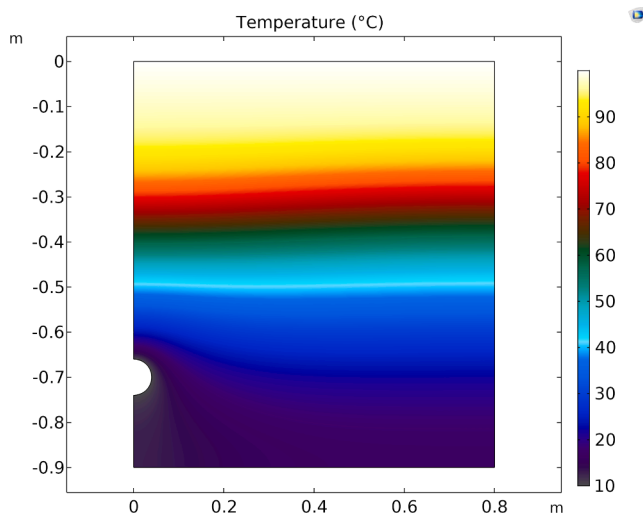**Fig. 40.** Temperature plot of steam treatment simulation after 5 simulated hours.

Fig. 41. Temperature plot of steam treatment simulation after 12 simulated hours.

Fig. 42. Temperature transients, comparison between radio wave and steam treatment.
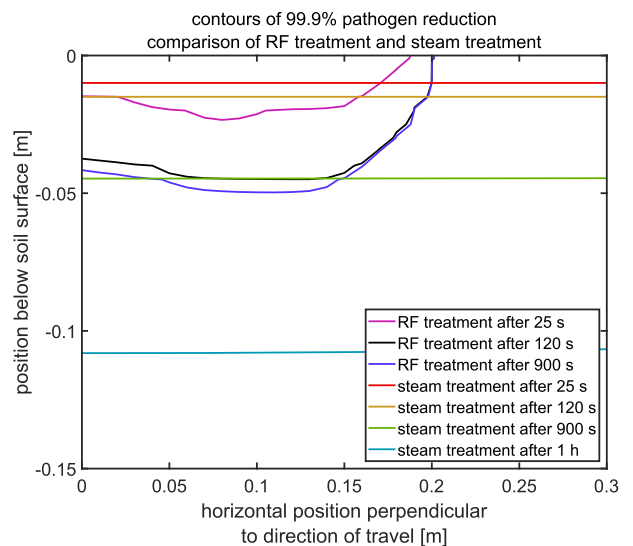
Fig. 43. Pathogen inactivation contours, radio wave versus steam treatment comparison.

(Fig. 43) accordingly present a similar difference in the onset of treatment effect. Radio wave treatment approaches its ultimate depth already in two minutes, while steam treatment takes fifteen minutes to reach this depth. This is faster than the aforementioned duration of about half an hour, likely because the pathogen inactivation dynamics are different between radio wave treatment and steam treatment. In particular, the duration of exposure to elevated temperature is longer than for radio wave treatment, so the threshold temperature is lower and can be reached in fifteen minutes. Nevertheless, this is still an order of magnitude longer than for radio wave treatment.

8. Discussion, radio wave treatment versus steam treatment

This section discusses the potential of radio wave treatment in comparison to steam treatment. On initial inspection, radio wave treatment exhibits faster dynamics, but shallower treatment depth. The distribution of the radio wave treatment efficacy may seem disadvantageous. Temperature decays with depth not unlike steam treatment, but this decay occurs over a much shorter distance than that of steam treatment does. However, this initial observation does not account for the additional potential that radio wave treatment may offer. Two

aspects on which radio wave treatment could provide notable benefits are discussed here: *selective application of treatment* and *supply chain integration*. The former of which implies a more precise application of heat where it is needed, and the latter a more efficient application of energy resources. Both aspects are subject to future design and development though, so no ultimate conclusions can be made at this present instance. Instead, several design considerations are presented here to make plausible that there indeed is opportunity for further improvement beyond the limitations of current treatment methods.

8.1. Selective application of treatment

As Sections 5.1 to 5.4 suggest, the efficacy of radio wave treatment can be improved through appropriate soil preparation. If one were to imagine a treatment case in which a specific pathogen needs to be suppressed over the root length of a specific crop, then the treatment requirement for this particular case would be to achieve 1) a threshold temperature, 2) down to a pre-determined depth, 3) with minimal temperature and depth overshoot to optimize energy utilization. Fig. 44

Fig. 44. Conceptual treatment case with three concept options: steam treatment (red, dash-dotted line), radio wave treatment with unaltered homogeneous soil (blue, dashed line), radio wave treatment with adjusted soil (green, solid line). (For interpretation of the references to color in this figure legend, the reader is referred to the web version of this article.)

illustrates this case with a graph of temperature (horizontal) versus the vertical position in soil (vertical). The temperature and depth requirements are indicated with dashed black lines.

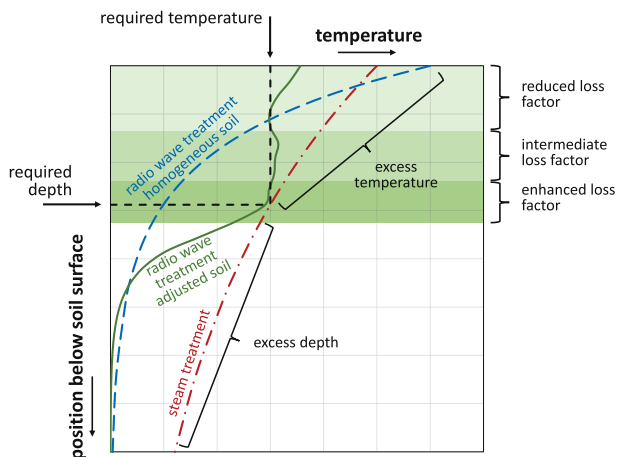Three treatment concepts are presented in this graph: 1) steam treatment (red, dash-dotted curve); 2) radio wave treatment with homogeneous unaltered soil (blue, dashed curve); and 3) radio wave treatment with soil that is prepared to locally adjust the dielectric properties to take advantage of the principle of selective heating (green, solid curve).

The curve for steam treatment has a minimum temperature of 100 °C at the soil surface, because this is the boiling point of steam. This temperature is higher than the required temperature threshold for pathogen inactivation, so at this position more heat is applied than required. Moreover, steam treatment is a slow process, so in the time it takes for the required temperature to develop at the required depth, heat will have transported to deeper soil layers beyond the required depth. This is in effect heat that is applied where it is not needed. This illustrates the unselectiveness of steam treatment, since more heat is applied to soil than required.

If instead radio wave treatment is applied without soil adjustment, then there is flexibility in the surface temperature. The radio wave field can in principle be regulated to heat soil to an arbitrary temperature. The depth of treatment in this case is limited though, because of the rate of decay of the radio wave field as it travels into soil.

The third and final conceptual case harnesses the selective heating principle to a greater extent by adjusting the soil prior to treatment. Three soil layers are drawn in the graph (Fig. 44): a top layer of reduced loss factor, which causes heat generation to be reduced despite this layer's proximity to the antenna; below this a second layer of intermediate loss factor; and finally the lowest treatment layer with an enhanced loss factor, which increases heat generation. The first, reduced loss layer could be created by loosening the top soil layer, or by allowing it to dry over a period of time. Furthermore, the third enhanced loss layer could be created by injecting water or an aqueous fertilizer solution at the appropriate depth.

In this manner, an optimum treatment recipe is envisioned. By making these soil adjustments prior to treatment, radio wave energy may be applied selectively to achieve the desired treatment effect at minimum energy expense. Specifically, the resulting solid green curve (Fig. 44) shows how the hypothetical optimized temperature profile may follow the lines that define the treatment requirement more closely than the other two treatment cases (dash-dotted red and dashed blue). Despite the fact that this is a hypothetical and unproven treatment

example, it demonstrates that radio wave treatment could offer greater flexibility than steam treatment in the application of energy to soil. Further principle designs could be conceived, but these are left for the consideration of subsequent development efforts.

8.2. Supply chain integration

Another relevant aspect to the development of radio wave treatment is supply chain integration. Two principle energy sources are considered in this context: fossil fuel and renewable sources. The overall efficiency for both radio wave treatment and steam treatment are considered each in relation to both energy sources.

For the case of steam treatment with fossil fuel, Appendix B provides figures for the overall energy flows. In that calculation the heat loss through the steam sheet corresponds to 7.9 % of the heating value of the natural gas that is combusted for steam generation. Moreover, the sensible heat of steam that is condensed into hot water onto the soil surface amounts to 9.1 % of the heating value of natural gas. This does not constitute a loss to the surrounding environment, but rather an amount of non-useful heat contained in condensation water that has no purpose after the latent heat of condensation has been released. Finally, the thermal losses of the boiler amounts to 28.5 %. The resulting efficiency is defined as heat that is usefully applied to the soil versus the lower heating value of natural gas. This efficiency is 54 %.

For the case in which fossil fuel is the energy source for radio wave treatment, electricity generated by combustion of natural gas is considered. In the Dutch context, gas fired power plants are reported to operate at an efficiency of up to 47 % (The International Energy Agency, 2008). The efficiency of converting electricity to radio wave energy with a 915 MHz magnetron is around 85 % (Meredith, 1998). Not including transmission losses, the overall efficiency of usefully applied heat versus the lower heating value of natural gas is 40 %.

For a non-fossil source, either renewable or nuclear, the assumption is made that an electrically heated boiler is much better insulated than a fossil fuel fired boiler. An efficiency of 100 % for converting electrical energy to steam is assumed. Only losses are considered due to heat losses through the steam sheet to the surroundings, and due to heat that is contained in non-useful condensation water. The resulting efficiency is 76 %. Finally, radio wave treatment with a renewable source is dictated by the efficiency of the magnetron, which was already mentioned to be 85 %.

A straightforward conclusion may seem to emerge; for a fossil fuel source, steam treatment has better efficiency; while for a renewable source, radio wave treatment has better efficiency. This becomes nevertheless more compounded when additional factors are included in the discussion. If indeed significant energy savings can be achieved by applying selective heating principles, then the energy balance will be more favorable for radio wave heating. Especially if the selective heating principle is harnessed by treating only localized patches of soil that show sign of infestation, which is a mode of operation that can flexibly be executed through radio wave treatment. Likewise, if fluctuations of a renewable non-fossil energy source need to be accommodated, then Section 5.7 suggests that this is expeditiously achieved through radio wave treatment. In contrast, steam treatment would not be as compatible with source fluctuations. A drop in available power directly results in a drop is steam flow, which may result in partial or complete sheet deflation and uneven treatment.

9. Conclusions

This study describes a simulation study on radio wave treatment of soil in glasshouse horticulture under parametric variation of physical variables. The model was developed as a framework model in a prior study, and it is adapted for this present study. The simulation environment is Comsol Multiphysics in combination with Matlab.

The simulation results show the following parametric dependencies.

Pre-treatment of soil enhances the effectiveness of the radio wave treatment process. Drying and loosening the soil to increase its porosity may therefore improve the depth of the treatment. Salinity variation also affects the treatment process, but it depends on the specific treatment case whether it is an advantageous or disadvantageous effect.

The effectiveness of radio wave treatment is determined by the short-term dynamics of radio wave heating rather than the long-term dynamics of transport of heat and moisture. Changing parameters related to these latter dynamics has little effect on the overall treatment process. In contrast, relevant parameters for the determination of treatment effectiveness are the dielectric properties of soil and its heat capacity, both are determined by soil composition and porosity.

Observations related to the process parameters are as follows. Increasing the power increases treatment depth. Varying the travel velocity of the antenna in proportion with the radio wave power, has little effect on the treatment effectiveness. Radio wave treatment can therefore in principle accommodate a fluctuating renewable energy source with no adverse effect to the treatment. Consequently, radio wave treatment of soil could potentially be deployed as a demand response application to balance supply and demand on the electrical grid.

The comparison to steam treatment is somewhat convoluted. Superficially, radio wave treatment is a much faster process than steam treatment, but it does not reach as deep into the soil. Moreover, it applies renewable sources more efficiently than steam treatment, but not fossil sources. Nevertheless, there remains room for design improvement of the radio wave treatment process to resolve its limitations, so this is no final verdict.

With the evolving energy landscape, and with the wide gap in technological maturity between the treatment methods, it is difficult to make any definitive conclusions. However, it indeed appears that radio wave treatment has the potential to be developed into a viable alternative for steam treatment.

CRediT authorship contribution statement

G.S.J. Sturm: Conceptualization, Methodology, Writing – original draft, Writing – review & editing. **A. van der Wurff:** Conceptualization, Resources. **S. Linnenbank:** Conceptualization, Resources. **J. Bonnet:** Conceptualization, Resources. **A. Koppert:** Conceptualization, Resources.

Declaration of competing interest

The authors declare that they have no known competing financial interests or personal relationships that could have appeared to influence the work reported in this paper.

Data availability

Data will be made available on request.

Acknowledgments

Appendix A—List of symbols

The list of symbols is presented in Table 2.

Table 2
List of symbols.

Symbol	Description	Symbol	Description
c_0	speed of light in vacuum	T	temperature
C_p	specific heat	t	time
$C_{p,a}$	specific heat of air	T_{av}	temperature of gas and vapor
$C_{p,s}$	dry specific heat of solids in soil	$T_{H_{v,0}}$	reference temperature for enthalpy of vaporization of water
$C_{p,wl}$	specific heat of liquid water	T_{sl}	temperature of solid and liquid
$C_{p,wv}$	specific heat of water vapor	T_{ref}	reference temperature for pathogen inactivation kinetics
$\mathbf{E}$	electric field vector component of the radio wave field	$u_0 \; \overline{u}_0$	vehicle velocity, vehicle velocity vector
E_a	activation energy for pathogen inactivation kinetics	$\overline{u}_l$	Darcy flow vector of liquid water In soil
f_{RF}	frequency of the radio wave field	V	arbitrary variable
f_A	function of Antoine equation that relates vapor pressure of water to temperature	$\widehat{V}$	smoothed arbitrary variable, indicated by caret
$\overline{g}$	gravitational acceleration vector	y	arbitrary variable
$H_{v,0}$	enthalpy of vaporization of water	α_s	smoothing parameter
ISM	Frequency bands available for Industrial, Scientific, and Medical purposes	α_T	turbulent diffusivity
k	permeability for Darcy flow	α_v	diffusivity of water vapor in air
k_0	vacuum wavenumber	α_w	diffusivity of moisture in soil
k_l	Darcy permeability for liquid water in soil	β_v	relaxation length
$k_{T_{ref}}$	rate constant of pathogen inactivation kinetics at reference temperature	ε'	real part of the complex relative permittivity
M_a	molecular weight of air	ε''	imaginary part of the complex relative permittivity
M_w	molecular weight of water	ε_0	permittivity of vacuum
n_a	molar bulk density of air in soil	ε_r	complex relative dielectric permittivity
N_L	pathogen population number on logarithmic scale	κ	thermal conductivity of soil
n_{wl}	molar bulk density of liquid water in soil	κ_{av}	thermal conductivity of air in porous volume of soil
n_{wv}	molar bulk density of water vapor in soil	κ_T	turbulent thermal conductivity
p	pressure	μ	dynamic viscosity of air/vapor
PDE	partial differential equation	μ_0	magnetic permeability of vacuum
Pr_T	turbulent Prandtl number	μ_r	complex relative magnetic permeability

Table 2 (*continued*)

Symbol	Description	Symbol	Description
p_v	vapor pressure of water	μ_T	turbulent viscosity
Q_{RF}	electromagnetic heat generation	μ_w	dynamic viscosity of liquid water
Q_v	heat of evaporation	ρ	density
$Q_{v,bc}$	heat of evaporation to surroundings in vicinity of soil surface	ρ_s	dry density of solids in soil
$Q_{\Delta T}$	sensible heat transfer	ρ_w	density of water
R	gas constant	τ	relaxation time of mixing
RF	radio frequency	τ_v	relaxation time constant
r_v	rate of evaporation	φ	relative porous volume
$r_{v,bc}$	heat of evaporation in vicinity of soil surface	φ_l	relative porous volume occupied by water
Sc_T	turbulent Schmidt number	ω	angular frequency of the radio wave field

Appendix B—Derivation of boundary conditions at soil surface for steam treatment

To simulate steam treatment, the boundary conditions at the top soil surface are modified to account for the transport of heat and moisture between soil and steam under the steam sheet. To this end, the turbulent flow patterns under the sheet are simplified first into a one-dimensional transport problem, and subsequently into a representation of two convective transport coefficients for heat and moisture with respect to bulk properties of the steam volume under the sheet.

It is arguably a considerable simplification to eliminate the interactions of the three-dimensional turbulent flow and the deformation of the flexible sheet in response to this flow. However, the focus in this study is primarily on physical interactions in soil, which justifies the simplification.

This appendix continues with two sections, in the first the overall mass and energy balances are established, and in the second the convective transport coefficients are derived.

B.1. Overall mass and energy balance

The treatment case involves steam generated by natural gas, applied for a period of 5 h, and a cumulative application of steam equivalent to 4 m³ of natural gas per m² of soil. As a basis for calculation the specifications of the S 2000 steam boiler from the company MSD GmbH (2020) are used to determine steam and heat fluxes and overall natural gas consumption. These manufacturer's specifications describe a different treatment case of treating 400 m² of soil over a 4 h period to a depth of 0.25 m and a temperature of around 80 °C. Despite this, their data allows for extrapolation to our case (4 m³ of natural gas per m² of soil) to quantify the overall energy and flux balances.

The S 2000 boiler is specified: to produce steam at a maximum rate of 2000 kg/h; to enable treatment of 90–100 m² of soil per our; and to consume 174 L of fuel oil per hour. With sensible heat and latent heat of evaporation of water and steam, this rate of steam production requires 1460 kW of thermal power, which aligns with the specified thermal output of 1500 kW. The corresponding energy expense is calculated to be 2042 kW from the lower heating value of fuel oil of 44 MJ/kg (0.96 kg/l) (The Engineering Toolbox, 2003e). Based on these figures the thermal losses in the boiler amount to 28 %.

For our treatment case (4 m³ of natural gas per m² of soil over 5 h) more thermal energy is required, but it is assumed that the boiler efficiency is the same. With the heating value for fuel oil that is mentioned above, and with the lower heating value of 31.6 MJ/m³ for natural gas according to Nederlandse Gasunie (1980), the respective energy expenses for combustion are calculated. These are 73.5 MJ/m² vs. 126.4 MJ/m², for the S 2000 specification vs. our treatment case. More thermal energy is expended, so a deeper treatment would result, and more steam is applied per unit area of soil. The steam consumption extrapolates to 34.5 kg/m² for our treatment case.

Losses to surroundings through the steam sheet are non-negligible. Ambient glasshouse temperature are elevated. For our case an ambient temperature of 40 °C is assumed. The convective heat transfer coefficient on the outside of the steam sheet is estimated by the method reported by McAdams (1954), referred to by Mills (1999) and data from The Engineering Toolbox (2003a). This method is used to calculate natural convection coefficient of a horizontal surface. This coefficient amounts to 10 W/m²K. With a temperature difference between sheet and ambient air of 100 °C – 40 °C = 60 °C, a heat loss to surroundings of 10 MJ/m² results.

B.2. Convective transport coefficients

The dominant gradients inside the steam sheet are over the shortest distance between soil and sheet, specifically the vertical direction. This justifies reduction of the transport phenomena to a one-dimensional problem, which implies a uniform distribution and perfect mixing in the horizontal plane.

The transport phenomena in the steam volume under the sheet are characterized by the turbulent viscosity. A quantification for the turbulent viscosity is obtained by first simulating three-dimensional turbulent flow in a geometry representing the steam sheet, and averaging the turbulent viscosity over this volume. In the simulated case, steam is fed every 10 m along a crop bed of 6.4 m with, into a steam sheet that is inflated to a height of 1 m. By employing symmetry, a simulated volume of 5 by 6.4 by 1 m represents the simulated case (Fig. 45). With the steam density calculated via the ideal gas law (0.54 kg/m³) and the steam consumption (34.5 kg/m²/5h = 1.9 g/m²s) the flow velocity through a 0.1 m diameter steam pipe amounts to 29 m/s, which is a practically feasible value for steam flow (Forbes Marshall, 2020). Applying appropriate boundary conditions, the Fluid Dynamics module of Comsol Multiphyisics is used to simulate the turbulent flow under the sheet; specifically, the k-ε turbulence model is used. The average turbulent viscosity (μ_T) that results from the simulation is 9.5 mPa·s.

From the average turbulent viscosity the other turbulent transport parameters are derived through the Reynolds analogy, specifically the turbulent diffusivity (α_T) and turbulent thermal conductivity (κ_T),

$$\alpha_T = \frac{\mu_T}{\rho Pr_T} = \frac{\mu_T}{\rho Sc_T} \tag{18}$$

$$\kappa_T = \frac{\mu_T C_p}{Pr_T} \qquad (19)$$

The turbulent Prandtl and Schmidt numbers are chosen following Kays and Crawford (1993) with both values at 0.85. The turbulent diffusivity amounts to $1.90 \cdot 10^{-2}$ m^2/s, and the turbulent thermal conductivity is 20.9 W/mK. These turbulent transport parameters are 850 resp. 450 times larger than their molecular counterparts for heat resp. mass transfer. Consequently, the molecular contributions (Hirshfelder, et al., 1954) to the transport phenomena are negligible and not included in this analysis.

The transport phenomena inside the sheet are thus reduced to a simple one-dimensional diffusion that applies to both heat and water vapor,

$$\partial_t y - \alpha_T \partial_z^2 y = \frac{y_{source} - y}{\tau} \qquad (20)$$

where y is an arbitrary variable. The source term on the right side derives from perfect mixing of the steam feed over the sheet volume. The symbol τ represents the corresponding time constant of mixing. The one-dimensional diffusion problem is solved as a coupled boundary value problem involving both the transfer of heat and water vapor. The temperatures at the soil and sheet positions are the primary variables, the partial vapor pressures at these positions equal the corresponding equilibrium vapor pressure. The curves for temperature and vapor pressure are defined by solving Eq. (20) to match these boundary value.

A solution in terms of the temperature at the soil level and the temperature at the sheet level is sought that satisfies the following conditions. Condensation occurs only at the sheet and soil surfaces, and the heat of condensation is released only at these positions. The flux of sensible heat into soil and through the sheet are derived from the gradient of the temperature curve, and the thermal conductivity. Equivalently, the flux of water vapor onto soil and onto the sheet is derived from the partial vapor pressure and the diffusivity. The condensation water that forms on the sheet falls onto the soil, so the flux of water into the soil is the sum of the vapor flux onto the soil and the flux onto the sheet. This combined flux of hot condensation water into the soil is equal to the specified steam consumption of 1.9 g/m^{2}s. The heat flux to ambient air is the sum of sensible heat and latent heat of condensation, this sum equates the heat flux based on temperature difference with ambient air and heat transfer coefficient.

Once a solution is found that satisfies these conditions, the convective heat and mass transfer terms can be calculated. The heat transfer coefficient into soil is the ratio between sensible heat flux and difference between average temperature and soil surface temperature; the mass transfer coefficient is ratio of total flux into soil and the vapor pressure difference between soil and saturated steam.

The resulting heat transfer coefficient is 71.56 W/m^{2}K with respect to a steam temperature of 99.5 °C. The mass transfer coefficient of 3.2 mm/s with respect to saturated steam. The release of latent heat due to the formation of condensation water is adjusted to account for heat losses through the sheet. In particular, as condensation water formed at the sheet falls on the soil, the associated heat of condensation escapes to ambient surroundings. This results in a lower effective heat of condensation that is applied to the soil in relation to the amount of condensation water that is introduced into it. The effective heat of condensation at the soil level is adjusted to 1954 kJ/kg.
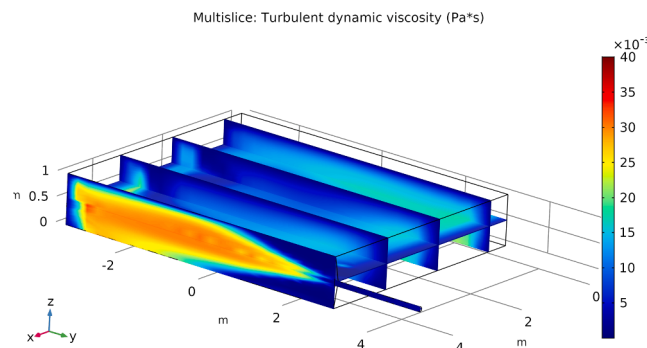

Fig. 45. Turbulence simulation under steam sheet.

References

Abbey, L., Udenigwe, C., Mohan, A., Anom, E., 2017. Microwave irradiation effects on vermicasts potency, and plant growth and antioxidant activity in seedlings of Chinese cabbage (Brassica rapa subsp. pekinensis). J. Radiat. Res. Appl. Sci. 10, 110–116. https://doi.org/10.1016/j.jrras.2017.01.002.

Agro Energy, 2017. De elektriciteitsmarkt in vogelvlucht in de tuinbouw. [Online]. Available at: https://www.agro-energy.nl/wp-content/uploads/2017/03/Whitepaper_Energie markt_in_vogelvlucht_LR.pdf. [Accessed 9 3 2020].

Avila, G., Faust, D., Kasevich, R. & Price, S., 1996. Demonstration of Radio-Frequency Soil Decontamination: KAI Technologies Demonstration (Volume III of III), s.l.: United States Air Force Armstrong Laboratory, available at https://apps.dtic.mil/sti/tr/pdf/ADA327886.pdf, accessed March 17th 2024.

Barker, K., Gooding, G., Elder, A., Eplee, R., 1972. Killing and preserving nematodes in soil with chemicals and microwave energy. J. Nematol. 4 (2), 75–79.

Bear, J., 1972. Dynamics of fluids in porous media. Dover Publications, New York.

Blanchard, C., Lyon, C. & Whitt, L., 1996. Demonstration of Radiofrequency Soil Decontamination: Volume I, s.l.: United States Air Force Armstrong Laboratory, available at https://apps.dtic.mil/sti/tr/pdf/ADA327889.pdf, accessed March 17th 2024.

Bollen, G., 1969. The selective effect of heat treatment on the microflora of a greenhouse soil. Neth. J. Plant Pathol. 75, 157–163. https://doi.org/10.1007/BF02137211.

Brodie, G., et al., 2007c. Evaluation of microwave soil pasteurization for controlling germination of perennial ryegrass (Lolium perenne) seeds. Plant Prot. q. 22 (4), 150–154.

Brodie, G., et al., 2015. Assessing the impact of microwave treatment on soil microbial populations. Glob. J. Agric. Innov., Res. Dev. 2 (1), 25–32. https://doi.org/10.15377/2409-9813.2015.02.01.3.

Brodie, G., et al., 2019. Understanding the Energy Requirements for Microwave Weed and Soil Treatment. Glob. J. Agric. Innov., Res. Dev. 6, 11–24. https://doi.org/10.15377/2409-9813.2019.06.2.

Brodie, G., et al., 2022. Microwave soil heating promotes strawberry runner production and progeny performance. Energies 15 (10), 3508. https://doi.org/10.3390/en15103508.

Brodie, G., Botta, C., Woodworth, J., 2007a. Preliminary investigation into microwave soil pasteurization using wheat as a test species. Plant Prot. Qtr. 22 (2), 72–75.

Brodie, G., Hamilton, S., Woodworth, J., 2007b. An assessment of microwave soil pasteurization for killing seeds and weeds. Plant Prot. q. 22 (4), 143–149.

Brodie, G., Ryan, C., Lancaster, C., 2012a. Microwave technologies as part of an integrated weed management strategy: a review. Int. J. Agron., 636905 https://doi.org/10.1155/2012/636905.

Brodie, G., Ryan, C., Lancaster, C., 2012b. The effect of microwave radiation on prickly paddy melon (Cucumis myriocarpus). Int. J. Agron., 287608 https://doi.org/10.1155/2012/287608.

Brodie, G., Khan, M., Gupta, D., 2020a. Microwave Soil Treatment and Plant Growth. In: Hasanuzzaman, M., Fujita, M., Teixeira Filho, M., Nogueira, T. (Eds.), Sustainable Crop Production. InTechOpen, London. https://doi.org/10.5772/intechopen.89684.

Brodie, G., Pchelnikov, Y., Torgovnikov, G., 2020b. Development of microwave slow-wave comb applicators for soil treatment at frequencies 2.45 and 0.922 GHz (Theory, Design, and Experimental Study). Agriculture 10 (12), 604. https://doi.org/10.3390/agriculture10120604.

Chen, Y., Gamliel, A., Stapleton, J., Aviad, T., 1991. Chemical, Physical, and Microbial Changes Related to Plant Growth in Disinfested Soil. In: Katan, J., DeVay, J. (Eds.), Soil Solarization. CRC Press, Boca Raton.

COMSOL AB, 2019. COMSOL Multiphysics 5.5. Stockholm:.

Conchado, A., Linares, P., 2012. The Economic Impact of Demand-Response Programs on Power Systems. A Survey of the State of the Art. In: Sorokin, A. (Ed.), Handbook of Networks in Power Systems i. Energy Systems. Heidelberg, Berlin.

Dabbene, F., Gay, P., Tortia, C., 2003. Modelling and control of steam soil disinfestation processes. Biosyst. Eng. 84 (3), 247–256. https://doi.org/10.1016/S1537-5110(02)00276-3.

Dev, H. & Sresty, G., 1996. Demonstration of Radiofrequency Soil Decontamination: Volume II of III, s.l.: United States Air Force Armstrong Laboratory, available at https://apps.dtic.mil/sti/pdfs/ADA327888.pdf, accessed March 17th 2024.

Science Direct, 2024. Advanced Search. [Online]. Available at: https://www.sciencedirect.com/search/entry. [Accessed 24 March 2024].

Edelstein, W., et al., 1994. Radiofrequency ground heating for soil remediation: science and engineering. Environ. Prog. 13 (4), 247–252. https://doi.org/10.1002/ep.670130413.

Eglitis, M., Johnson, F., 1970. Control of seedling damping-off in greenhouse soils by radio frequency energy. Plant Dis. Report. 54 (3), 268–271.

Eglitis, M., Johnson, F., Breakey, E., 1956. Soil pasteurization with high frequency energy (abstract). Phytopathology 46 (11), 635–636.

Falciglia, P., et al., 2018. A review on the microwave heating as a sustainable technique for environmental remediation/detoxification applications. Renew. Sustain. Energy Rev. 95, 147–170. https://doi.org/10.1016/j.rser.2018.07.031.

Fanti, A., et al., 2017. Nonlinear analysis of soil microwave heating: application to agricultural soils disinfection. IEEE J. Multiscale Multiphys. Comput. Tech. 2, 105–114. https://doi.org/10.1109/JMMCT.2017.2723264.

Ferriss, R., 1984. Effects of Microwave oven treatment on microorganisms in soil. Phytopathology 74 (1), 121–126. https://doi.org/10.1094/Phyto-74-121.

Griffin, G., Baker, R., 1991. Population Dynamics of Plant Pathogens and Associated Organisms in Soil in Relation to Infectious Inoculum. In: Katan, J., DeVay, J. (Eds.), Soil Solarization. CRC Press, Boca Raton.

Hess, M., et al., 2018. Microwave soil heating reduces seedling emergence of a wide range of species including invasives. Restor. Ecol. 26 (S2) https://doi.org/10.1111/rec.12668 (S160-S169).

Hess, M., Buisson, E., Mesléard, F., 2019. Soil compaction enhances the impact of microwave heating on seedling emergence. Flora 259, 151457. https://doi.org/10.1016/j.flora.2019.151457.

Hirshfelder, J., Curtiss, C., Bird, R., 1954. Molecular theory of gases and liquids. Wiley, New York.

International Telecommunication Union, 2020. Radio Regulations. [Online]. Available at: https://www.itu.int/dms_pub/itu-r/opb/reg/R-REG-RR-2020-ZPF-E.zip. [Accessed 19 9 2022].

Katan, J., DeVay, J. (Eds.), 1991a. Soil Solarization. CRC Press, Boca Raton.

Katan, J., DeVay, J., 1991b. Soil Solarization: Historical Perspectives, Principles, and Uses. In: Katan, J., DeVay, J. (Eds.), Soil Solarization. CRC Press, Boca Raton.

Kays, W., Crawford, M., 1993. Convective heat and mass transfer, 3rd ed. McGraw-Hill, New York.

Khan, M., et al., 2019. Impact of microwave disinfestation treatments on the bacterial communities of no-till agricultural soils. Eur. J. Soil Sci. 71 (6), 1006–1017. https://doi.org/10.1111/ejss.12867.

Khan, M.J., Brodie, G., Gupta, D., 2016. Effect of microwave (2.45 GHz) treatment of soil on yield components of wheat (Triticum aestivum L.). J. Microw. Power Electromagn. Energy. 50 (3), 191–200. https://doi.org/10.1080/08327823.2016.1228441.

Komarova, A., Likhacheva, A., Zvyagintsev, D., 2008. Influence of microwave radiation on soil bacteria. Mosc. Univ. Soil Sci. Bull. 63 (4), 190–195. https://doi.org/10.3103/S0147687408040078.

Koppert Machines, 2014. 20140327 koppertmachines agritron. [Online]. Available at: https://www.youtube.com/watch?v=Rdk4JZnOKig. [Accessed 24 1 2020].

Li, Q., et al., 2023. Effect of microwave treatment at 2.45 GHz on soil physicochemical properties and bacterial community characteristics in phaeozems of Northeast China. Agronomy 13, 600. https://doi.org/10.3390/agronomy13020600.

Forbes Marshall, 2020. Steam Pipes Sizing: Correct sizing of steam lines. [Online]. Available at: https://www.forbesmarshall.com/Knowledge/SteamPedia/Steam-Distribution/Steam-Pipe-Sizing. [Accessed 7 10 2020].

Mavrogianopoulos, G., Frangoudakis, A., Pandelakis, J., 2000. Energy efficient soil disinfestation by microwaves. J. Agric. Eng. Res. 75 (2), 149–153. https://doi.org/10.1006/jaer.1999.0492.

Maynaud, G., et al., 2019. Short-term effect of 915-MHz microwave treatments on soil physicochemical and biological properties. Eur. J. Soil Sci. 70 (3), 443–453. https://doi.org/10.1111/ejss.12769.

McAdams, W., 1954. Heat Transmission, 3rd ed. McGraw-Hill, New York.

Menges, R., Wayland, J., 1974. UHF electromagnetic energy for weed control in vegetables. Weed Sci. 22 (6), 584–590.

Meredith, R., 1998. Engineers' Handbook of Industrial Microwave Heating. Institution of Electrical Engineers, London.

Miler, N., Kulus, D., 2018. Microwave treatment can induce chrysanthemum phenotypic and genetic changes. Sci. Hortic., Issue 227, 223–233. https://doi.org/10.1016/j.scienta.2017.09.047.

Mills, A., 1999. Basic Heat & Mass Transfer, 2nd ed. Prentice-Hall, New Jersey.

Möschle Seifert Dämpftechnik GmbH, 2020. Steam boilers. [Online]. Available at: https://www.moeschle.de/en/steam-boilers. [Accessed 23 9 2020].

Nederlandse Gasunie, N.V., 1980. Basisgegevens Aardgassen. N.V. Nederlandse Gasunie, s.l.

Nelson, S., 1996. A review and assessment of microwave energy for soil treatment to control pests. Trans. ASAE 39 (1), 281–289. https://doi.org/10.13031/2013.27508.

Nelson, S., Stetson, L., 1974. Comparative effectiveness of 39- and 24S0-MHz electric fields for control of rice weevils in wheat. J. Econ. Entomol. 67 (5), 592–595.

NIST Chemistry Webbook, 2018. Water. [Online]. Available at: https://webbook.nist.gov/cgi/cbook.cgi?ID=C7732185&Units=SI&Mask=4#Thermo-Phase. [Accessed 5 2 2020].

O'Bannon, J., Good, J., 1971. Application of microwave energy to control nematodes in soil. J. Nematol. 3 (1), 93–94.

Pozar, D., 2005. Microwave Engineering, 3rd ed. Wiley, Hoboken.

Pullman, G., DeVay, J., Garber, R., 1981. Soil solarization and thermal death—a logarithmic relationship between time and temperature for four soilborne pathogens. Phytopathology 71 (9), 954–959. https://doi.org/10.4315/0362-028X-61.7.910.

Rahi, G., Rich, J., 2007. Potential of microwaves to control plant-parasitic nematodes in soil. J. Microw. Power Electromagn. Energy. 42 (1), 5–12. https://doi.org/10.1080/08327823.2007.11688574.

Rahi, G., Rich, J., 2011. Effect of moisture on efficiency of microwaves to control plant-parasitic nematodes in soil. J. Microw. Power Electromagn. Energy. 45 (2), 86–93. https://doi.org/10.1080/08327823.2011.11689802.

Roux-Michollet, D., Dudal, Y., Jocteur-Monrozier, L., Czarnes, S., 2010. Steam treatment of surface soil: how does it affect water-soluble organic matter, C mineralization, and bacterial community composition? Biol. Fertil. Soils 46, 607–616. https://doi.org/10.1007/s00374-010-0468-6.

Sabry, A., Allam, A., Abdel-Rahman, A. & El-Ansary, D., 2018. A Novel Microwave Applicator for Sandy Soil Disinfection. 2018 Progress In Electromagnetics Research Symposium (PIERS — Toyama), pp. 636-641, Doi: 10.23919/PIERS.2018.8597905.

Sahìn, H., 2014. Effects of microwaves on the germination of weed seeds. J. Biosyst. Eng. 39 (4), 304–309. https://doi.org/10.5307/JBE.2014.39.4.304.

Sartorato, I., Zanin, G., Baldoin, C., Zanche, C.D., 2006. Observations on the potential of microwaves for weed control. Weed Res. 46, 1–9. https://doi.org/10.1111/j.1365-3180.2006.00484.x.

Seaman, W., Wallen, V., 1967. Effect of exposure to radio-frequency electric fields on seed-borne microorganisms. Can. J. Plant Sci. 47, 39–49.

Staple, W., 1965. Moisture tension, diffusivity, and conductivity of a loam soil during wetting and drying. Can. J. Soil Sci. 45, 78–86. https://doi.org/10.4141/cjss65-010.

Sturm, G., et al., 2023. Numerical simulation framework for radio wave soil treatment for pathogen suppression. Comput. Electron. Agric. 211, 107992 https://doi.org/10.1016/j.compag.2023.107992.

Sun, X., et al., 2021. Simulations and experiments of the soil temperature distribution after 2.45-GHz Short-time term microwave treatment. Agriculture 11, 933. https://doi.org/10.3390/agriculture11100933.

Sun, X., et al., 2022. Simulations and experiments of soil temperature distribution after 2.45 GHz Long-term microwave treatment. Agriculture 12, 909. https://doi.org/10.3390/agriculture12070909.

Tadigiri, S., Chawla, G., Krishnan, P., 2016. Study on the effect of radiofrequency waves on root-knot nematode meloidogyne incognita. Indian J. Nematol. 46 (2), 126–139.

The Engineering Toolbox, 2003a. Air - Density, Specific Weight and Thermal Expansion Coefficient at Varying Temperature and Constant Pressures. [Online] . Available at: https://www.engineeringtoolbox.com/air-density-specific-weight-d_600.html. [Accessed 16 3 2020].

The Engineering Toolbox, 2003b. Air - Dynamic and Kinematic Viscosity. [Online]. Available at: https://www.engineeringtoolbox.com/air-absolute-kinematic-viscosity-d_601.html. [Accessed 5 2 2020].

The Engineering Toolbox, 2003c. Air - Thermophysical Properties. [Online]. Available at: https://www.engineeringtoolbox.com/air-properties-d_156.html. [Accessed 5 2 2020].

The Engineering Toolbox, 2003d. Water - Thermophysical Properties. [Online]. Available at: https://www.engineeringtoolbox.com/water-thermal-properties-d_162.html. [Accessed 5 2 2020].

The Engineering Toolbox, 2003e. Fuels - Higher and Lower Calorific Values. [Online]. Available at: https://www.engineeringtoolbox.com/fuels-higher-calorific-values-d_169.html. [Accessed 23 9 2020].

The Engineering Toolbox, 2004a. Air - Molecular Weight and Composition. [Online]. Available at: https://www.engineeringtoolbox.com/molecular-mass-air-d_679.html. [Accessed 5 2 2020].

The Engineering Toolbox, 2004b. Air - Specific Heat at Constant Pressure and Varying Temperature. [Online]. Available at: https://www.engineeringtoolbox.com/air-specific-heat-capacity-d_705.html. [Accessed 5 2 2020].

The Engineering Toolbox, 2004c. Steam Viscosity. [Online]. Available at: https://www.engineeringtoolbox.com/steam-viscosity-d_770.html. [Accessed 5 2 2020].

The Engineering Toolbox, 2005. Water Vapor - Specific Heat. [Online]. Available at: https://www.engineeringtoolbox.com/water-vapor-d_979.html. [Accessed 5 2 2020].

The Engineering Toolbox, 2010. Water - Heat of Vaporization. [Online]. Available at: https://www.engineeringtoolbox.com/water-properties-d_1573.html. [Accessed 5 2 2020].

The International Energy Agency, 2008. *Energy Efficiency Indicators for Public Electricity Production from Fossil Fuels.* [Online] . Available at: https://iea.blob.core.windows. net/assets/acaecb98-4430-4395-a4fa-d1a4d5ccb3d3/ EnergyEfficiencyIndicatorsforPublicElectricityProductionfromFossilFuels.pdf. [Accessed 21 1 2022].

The Mathworks, 2019. MATLAB, R2019b. Natrick.

Tkalec, M., et al., 2009. Effects of radiofrequency electromagnetic fields on seed germination and root meristematic cells of Allium cepa L. Mutat. Res./genet. Toxicol. Environ. Mutagen. 672 (2), 76–81. https://doi.org/10.1016/j. mrgentox.2008.09.022.

Velázquez-Martí, B., Gracia-López, C., 2004. Evaluation of two microwave surface distribution systems designed for substratum and agricultural soil disinfection. Span. J. Agric. Res. 2 (3), 323–331. https://doi.org/10.5424/sjar/2004023-87.

Warcup, J., 1951. Soil-steaming: a selective method for the isolation of ascomycetes from soil. Trans. Br. Mycol. Soc. 34 (4), 515–518. https://doi.org/10.1016/S0007-1536 (51)80035-4.

Wayland, J., Merkle, M., Menges, R., Robinson, R., 1975. Control of weeds with UHF electromagnetic fields. Weed Res. 15, 1–5. https://doi.org/10.1111/j.1365-3180.1975.tb01088.x.

Welle, A. v. d., 2016. *Ontwerp van elektriciteitsmarkten – benodigde aanpassingen voor een flexibeler energiesysteem op korte termijn.* [Online] Available at: https://repository. tno.nl/islandora/object/uuid%3A2df73fc0-25bf-4a83-a170-1349a66bef9d [Accessed 9 3 2020].

Wikipedia, 2019. *Mass diffusivity.* [Online] Available at: https://en.wikipedia.org/wiki/ Mass_diffusivity [Accessed 5 2 2020].

Wilde, M.D., et al., 2017. Using microwave soil heating to inhibit invasive species seed germination. Invasive Plant Sci. Manage. 10, 262–270. https://doi.org/10.1017/ inp.2017.29.